Earth-Science Reviews 216 (2021) 103523

Contents lists available at ScienceDirect

Earth-Science Reviews

journal homepage: www.elsevier.com/locate/earscirev

Review Article

Variability in the three-dimensional geometry of segmented normal fault surfaces

Vincent Roche [a,b,*], Giovanni Camanni [a,c], Conrad Childs [a,b], Tom Manzocchi [a,b], John Walsh [a,b], John Conneally [a,b], Muhammad Mudasar Saqab [d], Efstratios Delogkos [a,b]

[a] Fault Analysis Group, UCD School of Earth Sciences, University College Dublin, Belfield, Dublin 4, Ireland
[b] Irish Centre for Research in Applied Geosciences (iCRAG), UCD School of Earth Sciences, University College Dublin, Belfield, Dublin 4, Ireland
[c] DiSTAR, Università degli Studi di Napoli "Federico II", Naples, Italy
[d] Norwegian Geotechnical Institute, 40 St Georges Terrace, Perth, WA 6000, Australia

ARTICLE INFO

Keywords:
Normal faults
Fault segmentation
Fault geometry
Relay zone
Fault growth
3D fault geometry

ABSTRACT

Normal faults are often complex three-dimensional structures comprising multiple sub-parallel segments separated by intact or breached relay zones. Relay zones are classified according to whether they step in the strike or dip direction and whether the relay zone-bounding fault segments are unconnected in 3D or bifurcate from a single surface. Complex fault surface geometry is described in terms of the relative numbers of different types of relay zones to allow comparison of fault geometry between different faults and different geological settings. A large database of fault surfaces compiled primarily from mapping 3D seismic reflection surveys and classified according to this scheme, reveals the diversity of 3D fault geometry. Analysis demonstrates that mapped fault geometries depend on geological controls, primarily the heterogeneity of the faulted sequence and the presence of a pre-existing structure, as well as on resolution limits and biases in fault mapping from seismic data. Where a significant number of relay zones are mapped on a single fault, a wide variety of relay zone geometries occurs, demonstrating that individual faults can comprise segments that are both bifurcating and unconnected in three dimensions.

1. Introduction

Outcrop observation and mapping demonstrate that normal faults of all sizes are comprised of a series of segments (Goguel, 1952; Bristol and Treworgy, 1979; Larsen, 1988; Walsh and Watterson, 1990; Morley et al., 1990; Peacock and Sanderson, 1991; Delogkos et al., 2020). Early mapping of faults from seismic reflection surveys revealed the three-dimensional nature of fault segmentation (Childs et al., 1995; Mansfield and Cartwright, 1996; Kattenhorn and Pollard, 2001). Mapping of segmented fault arrays from high-quality 3D seismic reflection surveys is now routine, permitting detailed and extensive observation of the geometry of fault arrays (e.g. Childs et al., 2017; Freitag et al., 2017; Lăpădat et al., 2017; Collanega et al., 2019; Deng and McClay, 2019) and the distribution of displacement over them (e.g. Giba et al., 2012; Wilson et al., 2013; Duffy et al., 2015; Wrona et al., 2017; Ghalayini et al., 2017; Torabi et al., 2019).

Fig. 1 presents a selection of published fault surfaces interpreted mainly from 3D seismic reflection data. Fig. 1(L1-L4) shows four very different segmented fault arrays differentiated by whether the constituent segments are separated by strike relay zones (Fig. 1, L1 and L2) or dip relay zones (Fig. 1, L3 and L4), and whether the faults that bound the relay zones connect into a single plane (Fig. 1, L2 and L3) or are unconnected in 3D (Fig. 1, L1 and L4). Fig. 1(L5-L8) shows more complicated arrays with various combinations of different types of relay zone. These examples, and other recently published accounts of segmented fault arrays mapped from 3D seismic data (see Table 1), demonstrate that a wide range of fault geometries occur in nature. However, to date, there has been no attempt to combine these observations to obtain a general overview of 3D fault geometry. This paper aims to address this issue based on a large collection of faults and using a description of fault geometry based on the nature of the boundaries between the component fault segments. This catalogue permits comparison of the 3D geometry of fault surfaces from a range of different settings.

Fault geometries, such as those displayed in Fig. 1, are frequently related to the geological settings under which the faults formed. In particular, numerous studies have demonstrated significant impact of a

* Corresponding author at: Fault Analysis Group, UCD School of Earth Sciences, University College Dublin, Belfield, Dublin 4, Ireland.
E-mail address: vincent.roche@ucd.ie (V. Roche).

https://doi.org/10.1016/j.earscirev.2021.103523
Received 11 September 2020; Received in revised form 8 January 2021; Accepted 9 January 2021
Available online 14 January 2021
0012-8252/© 2021 The Authors. Published by Elsevier B.V. This is an open access article under the CC BY license (http://creativecommons.org/licenses/by/4.0/).

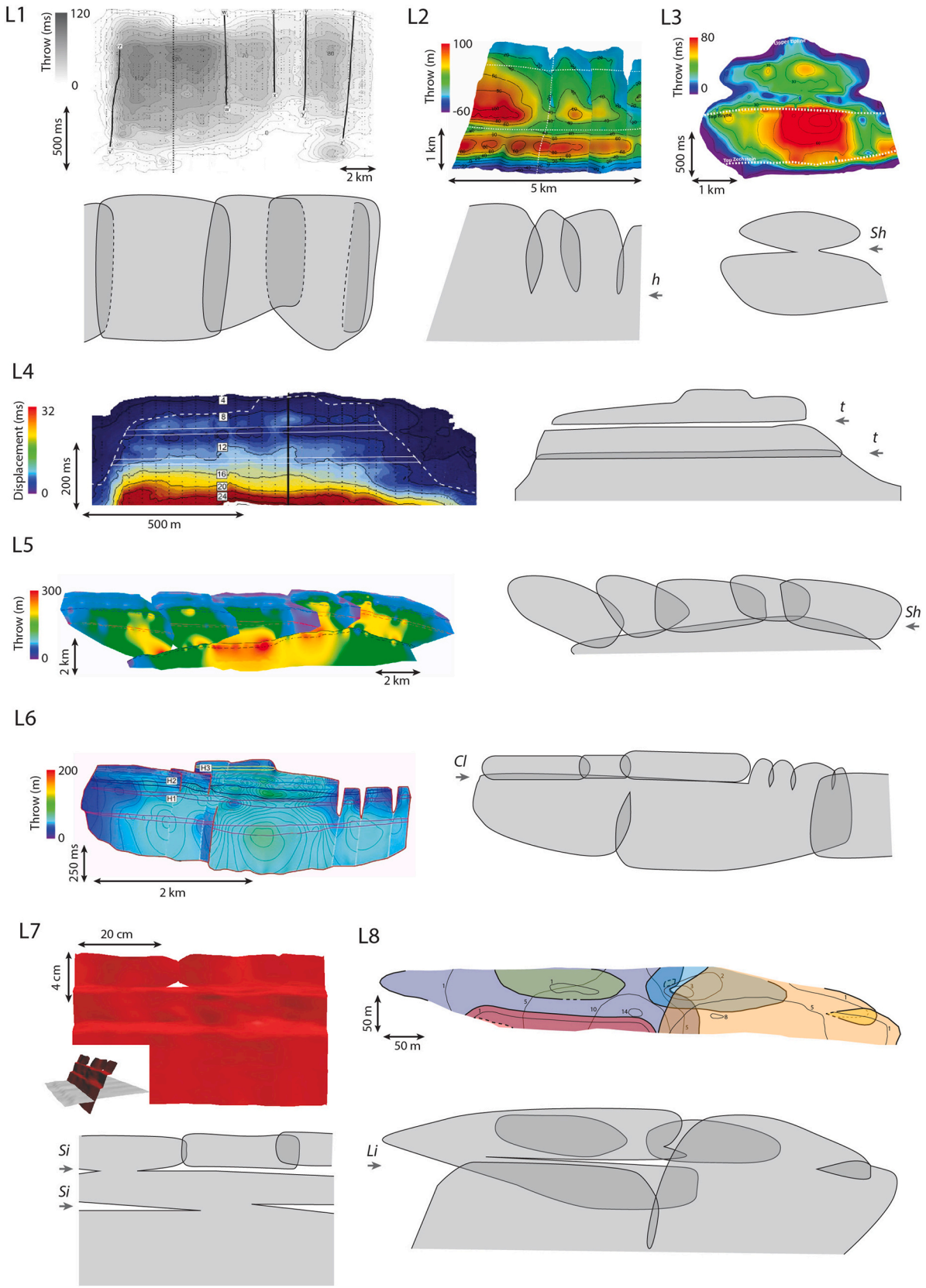

Fig. 1. Examples of fault surfaces from the literature. L1-L8: Labels of the faults. Modified from: (L1) Baudon and Cartwright (2008), (L2) Collanega et al. (2019), (L3) Tvedt et al. (2013), (L4) Seebeck et al. (2015), (L5) Deng et al. (2020), (L6) Lăpădat et al. (2017), (L7) Vasquez et al. (2018), (L8) Delogkos et al. (2020). In each case a strike-projection (usually coloured) is reproduced from the original paper, from which the simplified grey fault surface has been constructed to show our interpretation of the segmentation. The small grey arrows indicate the approximate levels of specific horizons influencing segmentation and discussed in the manuscript. Sh, h, t, Cl, Si and Li: names of the horizons (see text for details).

Table 1
Fault surface database.

Location	Ref.[a]	Name[b]	Fault geometry[c]					Tmax (m)[d]	Segmentation[e]					Geological controls[f]		
			S (km^2)	L (km)	H (km)	AR	Inc./ Com.		P. bif.	P. str.	P. right.	P. cont.	#	M. H.	S. I.	S. B.
East African Rift			29.9	12.7	2.5	5.1	0	175	0.86	1.00	0.60		7	0	1	0
			0.2	0.4	0.4	1.0	1	16	0.00	1.00	1.00		1	0	0	1
			1.4	1.5	1.1	1.4	1	38	0.71	0.57	0.25	0.67	7	0	0	0
		F16	8.5	6.2	1.9	3.3	1	63	0.73	0.65	1.00	0.83	15	0	1	0
			3.3	3.2	2.1	1.5	0	31	0.8	0.40	0.50	0.33	5	0	0	0
		F1	0.4	1.1	0.4	2.8	1	13	0.00	1.00	1.00		2	0	0	1
			2.0	1.8	1.4	1.3	0	19	0.43	0.29	0.00	0.40	7	0	0	0
			0.6	2.3	0.4	6.2	0	8	0.00	1.00	0.33		3	0	0	0
			0.3	1.3	0.3	4.3	1	14	0.00	1.00	0.00		2	0	0	1
			0.6	1.6	0.5	3.2	1	8	0.00	1.00	1.00		2	0	0	1
			0.9	1.2	1.1	1.1	0	20	0.60	0.40	1.00	1.00	5	0	0	0
			1.5	1.4	1.1	1.3	0	23	0.40	0.60	0.00	0.00	5	0	0	0
		F14	14.5	7.1	2.0	3.5	0	69	0.90	0.50	0.20	0.80	10	0	1	0
		F7	1.0	1.0	1.1	0.9	1	19	0.75	0.00		0.25	4	0	0	0
		F17	1.6	2.1	1.3	1.6	1	25	0.58	0.33	0.25	0.63	12	0	0	0
			0.5	0.9	0.8	1.1	1	16	0.50	0.50	0.00	0.00	2	0	0	0
			0.4	0.9	0.4	2.1	1	16	0.00	1.00	0.00		1	0	0	1
			0.9	1.3	0.8	1.7	1	15	0.50	0.50	0.33	0.67	6	0	0	0
			5.3	2.9	2.1	1.4	1	31	0.83	0.14	0.50	0.67	12	0	0	0
		F5	2.8	1.6	1.8	0.9	1	31	1.00	0.00		0.75	4	0	0	0
			5.8	3.8	1.9	2	0	56	0.75	0.42	0.20	0.57	12	0	0	0
			3.5	3.7	1.6	2.3	0	25	1.00	0.25	0.00	0.67	4	0	0	0
			0.7	0.9	1.1	0.8	1	19	1.00	0.50	1.00	0.00	2	0	0	0
African Atlantic Margin		F10	2.7	3.6	0.8	4.7	0	38	1.00	0.80	0.00	1.00	8	0	0	0
			2.3	3.2	0.7	4.2	0	44	1.00	0.86	0.17	1.00	4	0	0	0
			1.6	4.5	0.5	9.3	0	20	0.25	0.86	0.83	1.00	4	0	0	0
		F12	0.5	1.9	0.3	6.2	0	14	0.75	0.42	1.00	1.00	12	0	0	0
			0.4	2.5	0.2	13	0	13	0.50	0.73	0.63	1.00	8	0	0	0
			1.5	3.2	0.5	6.9	0	21	0.58	0.62	0.88	0.80	12	0	0	0
			2.6	5.4	0.4	14	0	16	0.75	0.70	0.86	1.00	8	0	0	0
			1.6	2.0	0.7	2.8	0	19	0.75	0.67	0.50	0.50	4	0	0	0
			2.0	2.5	0.7	3.8	0	16	0.53	0.38	0.00	0.69	19	0	0	0
			2.7	4.9	0.4	11	0	29	0.54	0.88	0.33	1.00	13	0	0	0
Bonaparte Basin			37.5	13.3	3.0	4.5	0	100	0.64	0.56	0.44	1.00	14	1	1	0
		F19	25.9	12.6	3.1	4.0	1	81	0.62	0.17	0.00	0.84	21	1	0	0
		F18	24.5	12.3	2.1	5.8	1	94	0.43	0.33	0.22	0.80	23	1	0	0
			16.0	8.5	2.1	4.0	1	74	0.65	0.26	0.33	0.75	20	1	0	0
Barents Sea			128.2	26.5	4.4	6.0	0	150	0.71	0.71	0.40	0.50	7	0	0	0
		F2	36.9	13.9	3.4	4.1	1	61	0.00	0.83	0.40	1.00	5	0	0	0
			32.2	13.1	3.3	4.0	1	75	0.00	1.00	1.00		1	0	0	0
			2.9	2.2	1.2	1.8	1	38	1.00	1.00	1.00		1	0	0	0
			63.8	19.1	2.6	7.3	0	163	0.60	0.58	0.67	1.00	10	0	0	0
			47.1	11.3	2.5	4.5	0	163	0.00	1.00	0.50		1	0	0	0
		F6	135.1	22.7	5.1	4.4	0	188	0.90	1.00	0.40		10	0	0	0
		F13	46	11.1	4.9	2.3	0	125	0.57	0.57	0.25	1.00	7	0	0	0
Porcupine Basin			9.1	11.7	0.9	12.6	1	71	0.57	0.92	0.33	1.00	7	0	0	1
		F4	15.6	12.2	1.4	8.8	0	94	0.67	1.00	0.50		6	0	0	1
			4.6	6.4	0.7	8.7	0	48	1.00	1.00	0.00		1	0	0	1
			2.6	4.3	0.7	6.3	0	55	1.00	1.00	0.25		2	0	0	1
			2.9	4.5	0.6	7.2	0	43	0.67	1.00	0.75		3	0	0	1
			5.0	5.0	1.2	4.1	0	68						0	0	1
			2.4	2.8	1.0	2.9	1	51	1.00	1.00	0.50		2	0	0	1
		F3	2.7	3.2	0.9	3.5	1	30	1.00	1.00	0.00		2	0	0	1
Molasse Basin		F20	2.6	3.2	0.9	3.7	0	28	0.26	0.52	0.17	0.64	19	1	1	0
Taranaki Basin		F11	82.4	16.9	5.2	3.2	0	128	0.82	0.84	0.00	1.00	11	0	1	0
South China Sea		F15	3.9	4.2	1.0	4.2	0	106	1.00	0.75	0.67	1.00	4	0	0	0
			3.7	3.8	1.2	3.2	0	68	1.00	1.00	0.00		1	0	0	0
		F9	2.6	2.4	0.9	2.5	0	25	0.50	1.00	0.33		2	0	0	0
			0.6	1.4	0.5	2.9	1	13	0.00	1.00	0.00		1	0	0	0
		F8	2.0	3.0	0.5	5.4	0	36	1.00	1.00	0.00		2	0	0	0
			1.0	2.0	0.8	2.6	0	25	0.00	1.00	0.50		2	0	0	0
			2.7	3.1	0.9	3.2	0	48						0	0	0
			0.5	1.9	0.3	5.5	1	23	1.00	1.00	0.00		1	0	0	0
Levant Basin	*(a)*	L1	14.0	14.0	1.0	14	0	125	0.00	1.00	0.00		3	0	0	0
Egersund Basin	*(b)*	L3	7.5	4.0	1.9	2.1	1	109	1.00	0.00		1.00	2	1	0	0
			5.6	3.0	1.9	1.6	0	227	1.00	0.00		1.00	2	1	0	0
			9.0	4.0	2.3	1.8	0	76	1.00	0.00		1.00	3	1	0	0
Analogue Model	*(c)*		0.0	0.0	0.0	2.0	0		0.50	1.00	0.50		2	0	0	0
Gulf of Gabes			0.5	1.5	0.3	5.0	0		1.00	1.00	0.00		2	0	0	0
			12.6	7.0	1.8	3.9	0		1.00	1.00	0.50		2	0	0	0
Niger Delta			4.0	3.3	1.2	2.8	0	130	0.33	0.33	0.00	0.50	3	0	0	0

(*continued on next page*)

Table 1 (*continued*)

Location	Ref.[a]	Name[b]	Fault geometry[c]					Tmax (m)[d]	Segmentation[e]					Geological controls[f]		
			S (km^2)	L (km)	H (km)	AR	Inc./ Com.		P. bif.	P. str.	P. right.	P. cont.	#	M. H.	S. I.	S. B.
Northern N. Sea			10.0	5.0	2.0	2.5	0		1.00	1.00	0.33		3	0	0	0
Suez Rift	*(d)*		240.0	40.0	6.0	6.7	0	500	0.00	0.57	0.88	1.00	14	1	1	0
E. Denmark	*(e)*		0.0	0.0	0.0	0.4	0	<1	0.50	0.25	1.00	0.33	4	0	0	0
Inner Moray Firth	*(f)*	L6	8.0	4.0	2.0	2.0	1	250	0.36	0.73	0.38	1.00	11	1	0	0
Basin			42.0	14.0	3.0	4.7	0	450	0.60	1.00	0.00		5	1	0	0
Petrel Sub-basin	*(g)*	L4	0.4	1.0	0.4	2.7	0	40	0.00	0.00		1.00	2	0	0	1
Porcupine Basin	*(h)*		4.5	4.0	1.1	3.6	0	150	1.00	1.00	1.00		4	0	1	0
Ptolemais Basin	*(i)*	L8	0.1	0.6	0.2	4.0	0	19	0.50	0.50	0.75	1.00	8	1	0	0
Columbus Basin	*(j)*		8.0	4.0	2.0	2.0	0	250	1.00	1.00	1.00		6	0	0	0
Analogue model	*(k)*	L7	0.0	0.0	0.0	3.2	0	<1	0.50	0.25	0.00	1.00	8	1	0	0
Taranaki Basin	*(l)*		15.0	7.5	2.0	3.8	1	50	0.00	1.00	0.00		1	0	1	0
			10.0	5.0	2.0	2.5	0	40	0.50	1.00	0.50		2	0	1	0
		L2	15.0	5.0	3.0	1.7	0	100	1.00	1.00	0.00		3	0	1	0
			12	4.0	3.0	2.0	0	60	1.00	0.00		1.00	2	0	1	0
Enderby Terrace	*(m)*		350.0	35.0	10.0	3.5	0	2000	0.00	0.55	1.00	1.00	8	1	1	0
	(n)	L5	120.0	20.0	6.0	3.3	0	300	0.00	0.44	0.00	1.00	9	1	1	0

[a] Data for the literature faults from: (a) Baudon and Cartwright (2008), (b) Tvedt et al. (2013) (C3, C4, C2)*, (c) Marchal et al. (2003) (F1, F7, F2, F6, Fz)*, (d) Jackson and Rotevatn (2013), (e) Kristensen et al. (2008) (Fig. 5)*, (f) Lăpădat et al. (2017) (Fig. 10, Fig. 9)*, (g) Seebeck et al. (2015), (h) Worthington and Walsh (2017) (Fig. 10)*, (i) Delogkos et al. (2020), (j) Freitag et al., 2017 (F1)*, (k) Vasquez et al. (2018), (l) Collanega et al. (2019) (F1/2, F3/5, F7, F6)*, (m) Deng and McClay (2019), (n) Deng et al. (2020). *: The names and figures inside the brackets refer to the associated publications

[b] Name of the faults in Figs. 1 and 6.

[c] S: Fault surface area; L: Fault length measured in the strike dimension; H: Fault height measured in the dip dimension; AR: Fault surface aspect ratio; Inc./Comp: incomplete fault (0), complete fault (1).

[d] Tmax: estimated maximum throw.

[e] P. bif.: Proportion of bifurcating relay zones; P. str.: Proportion of strike relay zones; P. right.: Proportion of right-stepping relay zones; P. cont.: Proportion of contractional relay zones; #: number of bifurcating and cylindrical relay zones.

[f] (1) indicates a mechanical heterogeneity (M.H.), an underlying structural inheritance (S.I.) and a stratabound fault (S.B.), (0) indicates that these settings are not recognised.

weak layer in the faulted sequence in promoting the formation of dip relay zones (Childs et al., 1996a; Schöpfer et al., 2006; Jackson and Rotevatn, 2013; Lăpădat et al., 2017; Vasquez et al., 2018; Deng and McClay, 2019) and of a reactivated underlying structure on the formation of strike relay zones between fault segments with a bifurcating geometry (Giba et al., 2012; Worthington and Walsh, 2017; Collanega et al., 2019). The catalogue of segmented faults presented here (see Table 1) is based primarily on faults mapped from eight 3D seismic surveys, but also incorporates data derived from published accounts such as those in Fig. 1. It covers a range of different geological settings, permitting a general overview of the first-order controls on fault zone geometry in three-dimensions.

As well as presenting results from newly mapped faults, this paper draws extensively from previously published examples of fault surfaces and the ideas presented in them. The large database of fault surfaces provides a basis for a general description of fault surface geometry in 3D and for considering the constraints that 3D geometry may place on models of fault growth. Different fault geometries have in the past promoted different models of how faults evolve (Childs et al., 1996b; Walsh et al., 2003). For example the series of unconnected fault segments in Fig. 1(L1) may suggest that initially isolated fault segments grew towards one another to form a segmented array, while Fig. 1(L2) may be interpreted to indicate that segmentation arose by bifurcation of an upward propagating fault. By providing a broad overview of fault geometry, this paper provides a basis for considering how fault geometry constrains models of fault development. Furthermore, our mapping and the data derived from the literature are subject to the inherent and irreducible resolution limits that place constraints and biases on fault mapping from seismic reflection data. The impact of these on our results and on the use of seismic data for constraining models of fault geometrical evolution are considered.

It is intended that the generalised description of the 3D geometry of fault arrays can be of value for many practical applications, for example to better evaluate fault controls on the flow of mineralising fluids in ore systems and of hydrocarbons within faulted reservoirs (e.g. Rotevatn et al., 2007; Manzocchi et al., 2008; Micklethwaite et al., 2015; Walsh et al., 2018; Kyne et al., 2019), or the initiation and termination of earthquake ruptures (Das and Aki, 1977; Segall and Pollard, 1980; Machette et al., 1991; Stein et al., 1997; Soliva et al., 2008; Wesnousky, 2008; Pizzi et al., 2017; Oglesby, 2020).

2. Approach to fault parameterisation

2.1. Parameterization of relay zones

To compare the geometry of individual segmented faults we parametrize them based on the "form" and "orientation" of the relay zones that separate their segments, following the terminology of Camanni et al. (2019) (Fig. 2). Two forms of relay zone are distinguished: (i) relay zones that are bound by segments that merge to a single surface (e.g. Clayton, 1966; Segall and Pollard, 1980; Jackson, 1987; Childs et al., 1995; Huggins et al., 1995; McGrath and Davison, 1995; Walsh et al., 1999; Freitag et al., 2017) referred to as bifurcating relay zones, and (ii) relay zones that are bounded by segments that are unconnected in three dimensions (e.g. Childs et al., 1995; Baudon and Cartwright, 2008; Long and Imber, 2011) referred to as cylindrical relay zones (Fig. 2). Other forms of relay zones (e.g. double-bifurcating) also exist in nature (Camanni et al., 2019), but are relatively uncommon and are not considered here.

There are two end-member relay zone orientations: (i) relay zones where the bounding segments step along the fault strike (e.g. Childs et al., 1995; Huggins et al., 1995; Marchal et al., 2003; Baudon and Cartwright, 2008; Long and Imber, 2011) referred to as strike relay zones and (ii) relay zones which step in the dip direction of the fault (e.g. Childs et al., 1996a; Mansfield and Cartwright, 1996; Walsh et al., 1999; Kattenhorn and Pollard, 2001; Kristensen et al., 2008; Tvedt et al., 2013) referred to as dip relay zones. Strains at strike relay zones are volumetrically neutral for normal faults, i.e. with a screw dislocation type of

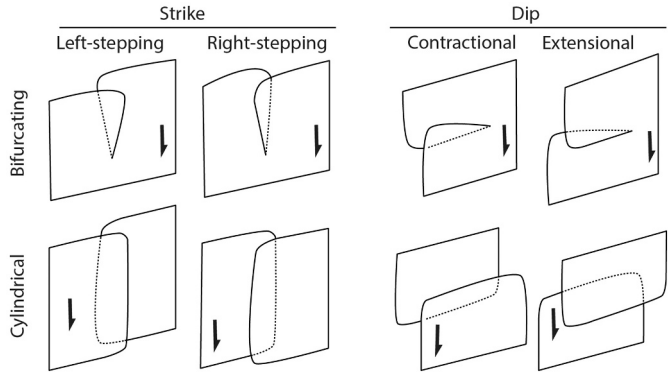

Fig. 2. Main geometries of relay zones observed on fault surfaces, which can be reduced into four types: bifurcating strike relay, bifurcating dip relay, cylindrical strike relay and cylindrical dip relay.

discontinuity that forms a characteristic relay ramp in horizontally layered sequences (Larsen, 1988). For this reason, relay zones with these orientations have been referred to previously as neutral relay zones (e.g. Walsh et al., 1999; Camanni et al., 2019; Delogkos et al., 2020). By contrast, strains at dip relay zones accommodate an edge dislocation type of discontinuity that can be either contractional or extensional in restraining and releasing relay zones, respectively. Relay zones are identified here as either dip or strike despite many "oblique" relay zones having intermediate orientations. This relatively crude categorisation is used to simplify relay zone parameterisation and is reasonable as oblique relay zones mapped from seismic data are significantly less common than strike and dip relay zones (Camanni et al., 2019). A pitch of 45° for the relay axis is used as a threshold value to differentiate strike and dip relay zones (see Camanni et al., 2019). The terms strike and dip relay zones are equivalent to the "displacement-parallel" and "displacement-normal" relay zones used in previous studies (e.g. Peacock and Sanderson, 1991).

Based on form and orientation, three-dimensional relay zone geometries can therefore be subdivided into four categories: bifurcating strike, bifurcating dip, cylindrical strike and cylindrical dip relay zones (Fig. 2). It is important to note that the form and orientation of a relay zone are the same irrespective of whether it is breached or not. For example, a fault that bifurcates from one surface into two, does so irrespective of whether the two fault segments are separated from one another by an intact relay zone or are connected along a branch-line(s) (see Walsh et al., 1999; Camanni et al., 2019). The categorisation is also independent of the stepping direction between the bounding segments, insofar as dip relay zones can be either contractional or extensional and strike relay zones can be either left- or right-stepping.

2.2. Parameterisation of fault surfaces

We describe the geometries of individual faults as the proportion of relay zones on the fault that are strike, as opposed to dip, and the proportion that are bifurcating, as opposed to cylindrical, so that each fault can be represented as a point on a cross-plot of proportion of strike relay zones versus proportion of bifurcating relay zones (Fig. 3). The outer limits of this diagram correspond to a range of simple segmented fault geometries. End-member geometries of segmented faults comprising relay zones that all have the same form and orientation are located in the four corners of the graph. The segmented faults that plot on the lower horizontal axis comprise all cylindrical relay zones with a range of orientations from all strike (lower right-hand corner) to all dip (lower left-hand corner) relay zones. The segmented faults that plot on the upper horizontal axis define an equivalent spectrum of fault structure but with all bifurcating relay zones. The segmented fault that plots in the centre of the diagram shows a more complex mixture of relay zone form and orientation. By locating many faults on this plot, we can distinguish between the segmentation characteristics of fault surfaces of different size, shape and geological setting.

This parameterisation is based on the numbers of different types of relay zone on a fault surface. These numbers are relatively easy to measure from 3D fault mapping and can be defined objectively as we consider a relay zone as the region between two adjacent segments and we do not, for example, group segments together to define larger scale relay zones. This point is illustrated by Fig. 1(L5) that comprises six fault segments, five segments in the upper half of the fault and one in the lower half. The upper five segments are separated by four cylindrical strike relay zones and they are each separated from the lower segment by a cylindrical dip relay zone so that a total of nine relay zones are identified for this fault. There are rare instances where we record two relay zones between two fault segments where the tip-lines bounding the relay zone bend so that a strike relay zone gives way to a dip relay zone. An example of this geometry is illustrated by the upper left-hand corner of the fault in Fig. 1(L6).

3. Fault data

3.1. Fault surface database

The compiled fault surface database comprises data derived both from published fault surface maps and from eight seismic reflection surveys interpreted for this purpose. The main geometrical attributes of all faults within the database are given in Table 1.

The 63 newly-mapped fault zones used in this study have been mapped using inline and cross-line interpretation, horizon tracking and seismic attributes, with detailed mapping of all seismically resolvable relay zones. An example of a seismic line for each area is presented in Fig. 4 to illustrate the quality of the data. Two of the seismic datasets are depth migrated. For the six datasets in time domain, the fault throws and the down-dip dimensions were converted to depth using a multiplier of 1.25 (i.e. a constant velocity of 2500 m/s), a value which is within c. 10% of the estimated average velocities for the sequences and depth ranges of the individual datasets.

The mapped fault zones are referred to as "complete" where they are entirely covered by the seismic survey and bounded in all directions either by tip-lines or by branch-lines with faults of a different orientation. They are referred to as "incomplete" when they extend beyond the limits of the resolvable seismic data (*Inc./Com.* in Table 1). The faults have surface areas (*S* in Table 1) between 0.2 and 200 km^2 and offset sub-horizontal sedimentary layering with throws generally between 10 m and 100 m (*T* in Table 1, Fig. 5a). With a few exceptions in the East African Rift, the faults have larger along-strike (*L* in Table 1) than down-dip dimensions (*H* in Table 1) (Fig. 5b). The mapped fault surface aspect ratio (*AR* in Table 1) is defined as the along-strike to down-dip dimension ratio (*L/H*) and ranges from 0.8 to 14. This variability in aspect ratio may either be a

consequence of sampling or of underlying geology, but in either case may influence the proportions of relay zones of different types that may be observed on the faults. This topic will be returned to in Section 4.3.

Examples of the outlines of 20 mapped segmented faults are presented in Fig. 6. Between them, these contain 179 relay zones of various types. In total, 510 individual relay zones have been counted on all of the newly-mapped faults. Among these, 408 are cylindrical or bifurcating relay zones, but 102 relay zones have not been categorised as either bifurcating or cylindrical because they are not entirely contained within the seismic volume (41), or have a double-bifurcating (20), or more complex geometry (41). Hence about 20% of the total number of relay zones cannot be included in the calculation of the relative proportions of bifurcating and cylindrical relay forms. All the mapped relay zones are used to calculate the proportion of strike relay zones, including those that extend beyond the seismic volume. Two of the 63 faults do not contain any relays identifiable as either bifurcating or cylindrical, and hence are not included in the analysis of the proportion of relay zones. The other faults each contain up to 23 bifurcating or cylindrical relay zones (Table 1). While we have mapped equal proportions of left- and right-stepping strike relay zones, contractional relays are much more common than extensional ones (Table 1) (Camanni et al., 2019). The smallest relay zones mapped have separations as low as 20 m for the highest resolution data. In the lower-resolution datasets (from the Barents Sea, Porcupine Basin and Taranaki Basin) minimum mapped separation was 40 m. The largest mapped relay zones have a separation of about 1000 m. The majority of the relay zones are bounded by segments that overlap in 3D, but there is also a proportion of relay zones (24%) that are bounded by underlapping fault segments (see Camanni et al., 2019 and Childs et al., 2017 for analyses of those geometries).

The 24 fault zones compiled from the literature are derived from seismic reflection data (Marchal et al., 2003; Baudon and Cartwright, 2008; Jackson and Rotevatn, 2013; Tvedt et al., 2013; Seebeck et al., 2015; Worthington and Walsh, 2017; Freitag et al., 2017; Lăpădat et al., 2017; Collanega et al., 2019; Deng and McClay, 2019; Deng et al., 2020), field observations (Kristensen et al., 2008; Delogkos et al., 2020) and sandbox models of normal faulting (Marchal et al., 2003; Vasquez et al., 2018). The same geometrical attributes as those described above for the newly-mapped faults are given in Table 1. These "literature faults" have been selected as they describe large parts of faults that were interpreted in 3D for the purpose of studying fault geometry and therefore are suited to parameterisation. Published accounts of limited areas of faults centred on individual relay zones (e.g. Childs et al., 1995; Long and Imber, 2011; Conneally et al., 2014) and faults for which interpretations of the form and orientation of the relay zones are uncertain (e.g. Kattenhorn and Pollard, 2001; Giba et al., 2012; Wilson et al., 2013) have not been included in the database. The faults that have been included are parameterised based on published maps, cross-sections and fault surface maps (strike-projections) and on descriptions of the faults provided in the various publications. Selected examples of published fault surface maps and simplified versions of these maps on which our parameterisation is based are illustrated in Fig. 1. This parameterisation is based only on the published papers and our understanding of them, and it may be that additional data or discussion with the authors could modify these parameters. An example of subjectivity in interpretation is the fault surface shown in Fig. 1(L6), which, as published, does not explicitly show any dip relay zones. However, it appears from the associated paper (Lăpădat et al., 2017) that the authors identify breached dip relay zones, which are represented in the simplified version of this fault surface.

Faults from the literature contribute a total of 109 relay zones to the database, with up to 14 on a single fault. These data are included to broaden the scope of our analysis but they are excluded from our plots involving relay separation (see Sections 4.2 and 7.1), because that attribute is not provided in the relevant publications.

3.2. Geological settings of the mapped faults

The newly-mapped faults are located in eight different sedimentary basins including the Bonaparte Basin offshore northwest Australia (Saqab and Bourget, 2015), the Porcupine Basin offshore West of Ireland (Worthington and Walsh, 2017), the Taranaki Basin offshore western New Zealand (Giba et al., 2012) and the Alps foreland Molasse Basin in NE Switzerland (Marchant et al., 2005). The precise location of the other

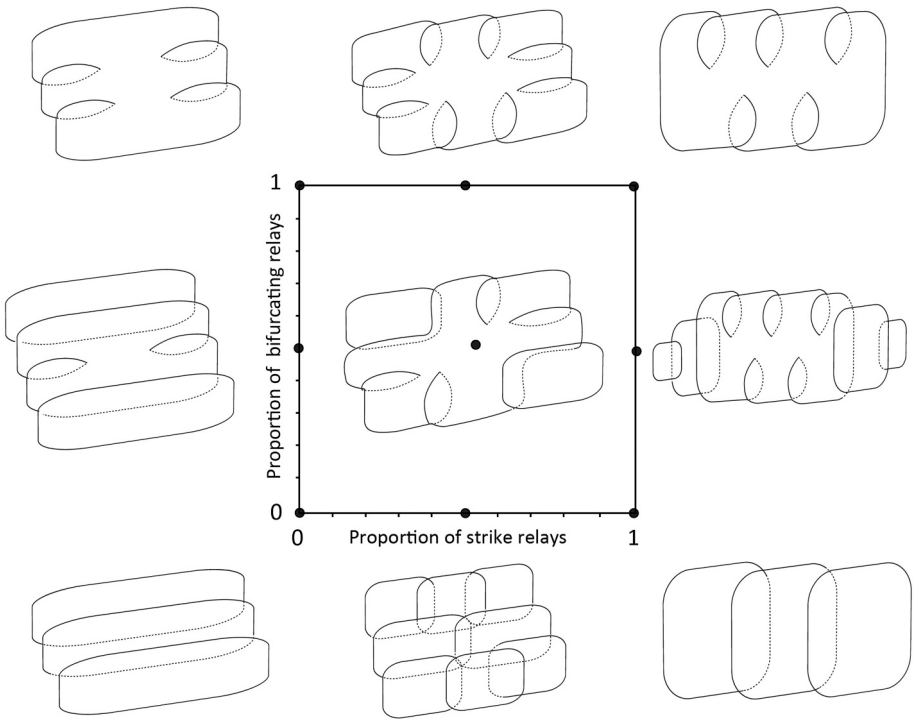

Fig. 3. Conceptual geometries of 3D segmentation with different proportions of the four main types of relay zones. These geometries are located in different positions on the diagram showing the proportion of bifurcating relays as a function of the proportion of strike relays.

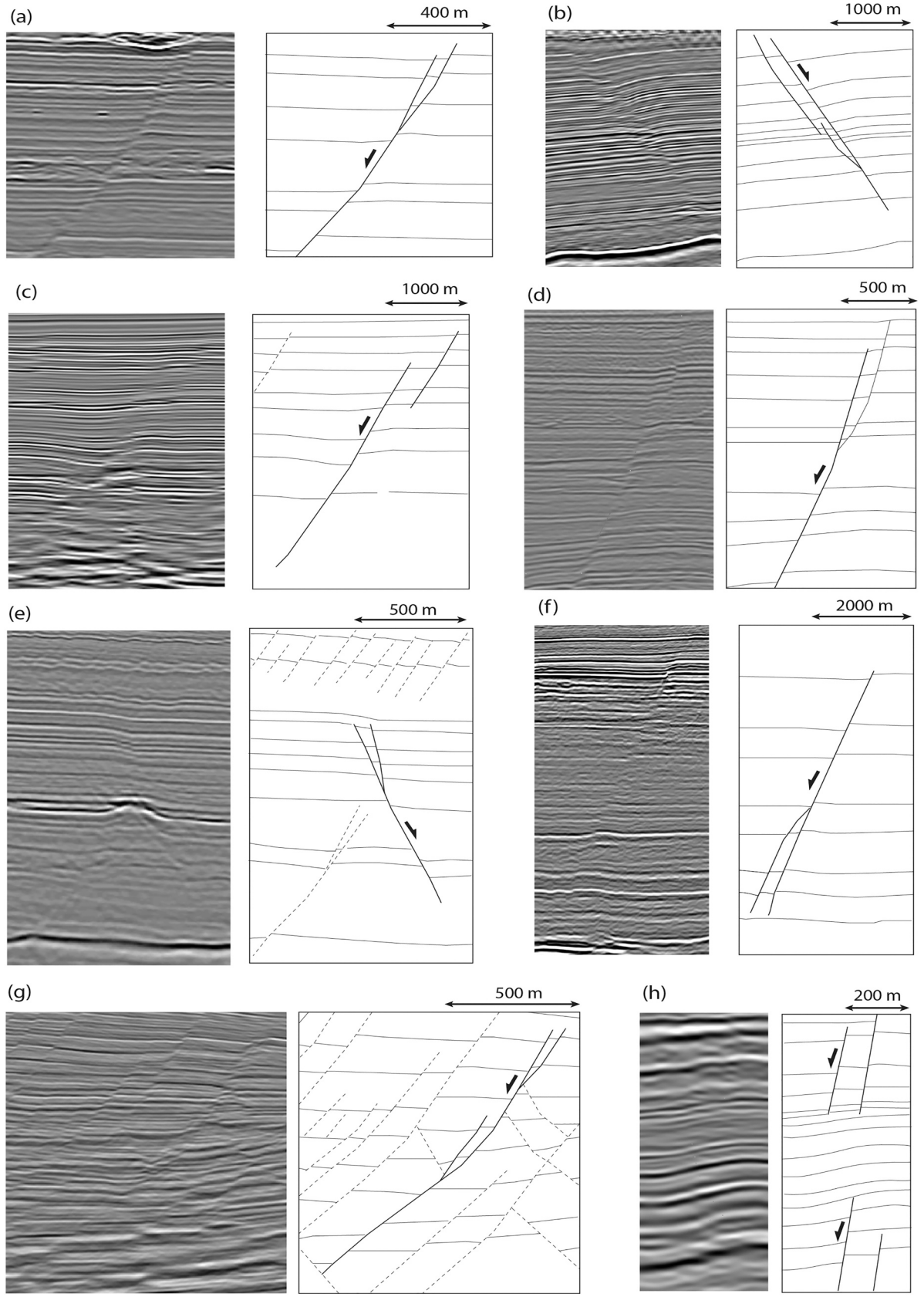

Fig. 4. Examples of seismic sections through segmented fault surfaces studied in each dataset. (a) African Atlantic Margin. (b) East African Rift. (c) Bonaparte Basin. (d) Taranaki Basin. (e) Porcupine Basin. (f) Barents Sea. (g) South China Sea. (h) Molasse Basin. The locations of the sections relative to the fault surfaces are indicated in Fig. 6. Thick line: fault trace; thin line: horizon; dashed line: fault trace that does not belong to the studied fault zones. Each section is presented with an approximately 1:1 vertical to horizontal scale.

four datasets is confidential but they are from the African Atlantic Margin, the Barents Sea, the East African Rift and the South China Sea (Table 1). The mapped faults are generally young (Cenozoic), at shallow depths (less than 1.5 km) and in areas of low strain (less than c. 15% extension). The only exception is the Barents Sea dataset for which Early Cretaceous faults are mapped to depths of 5 km. The individual study areas often have complex structural histories with several faulting episodes which are not detailed here. Instead, the settings specified below and in Table 1 refer to the deformation history of the mapped faults only, emphasising the three geological controls considered to have the highest impact on 3D fault segmentation. These controls are: (1) underlying structural inheritance, (2) mechanical heterogeneity and (3) whether the faults are stratabound (Table 1, *S.I., M.H.* and *S.B.*). The three controls are considered as qualitative, binary selections in Table 1: either the control is considered to have been influential, or it is not. The criteria for making these choices are outlined below.

Faults that are said to have an underlying structural inheritance (Table 1, *S.I.*) are those that are either directly connected to, or spatially associated with, a pre-existing structure that is reactivated during later extension. In this setting, fault surfaces can twist upward to form segmented en-echelon arrays in the cover above the older structure as seen from seismic mapping (Giba et al., 2012; Worthington and Walsh, 2017; Collanega et al., 2019) and analogue modelling (Corti, 2008; Clifton et al., 2000). Underlying structural inheritance is considered important (*S.I.* = 1 in Table 1) for several of the studied faults. The fault mapped within the Mesozoic sequence of the Molasse Basin has a geometry controlled by oblique reactivation of an underlying fault during a Miocene episode of extension (Roche et al., 2020). A Neogene aged fault mapped in the Taranaki Basin is mainly attributed to a deeper pre-existing Cretaceous fault (see Giba et al., 2012; Conneally et al., 2017). In the Bonaparte Basin, of the four Neogene age faults studied, one connects downwards to an earlier Mesozoic fault, whereas the others do not; see Saqab and Bourget (2015) for a detailed description of similar types of faults. Similarly, in the East African Rift, three large faults developed above a reactivated pre-existing structure while 20 smaller faults are not associated with underlying faults. For the other mapped areas, the influence of a pre-existing structure is considered to be moderate to absent (i.e. *S.I.* assigned a value of 0 in Table 1), meaning either: (a) there is no pre-existing structure observed locally, (b) the faults are entirely decoupled from any pre-existing structure, (c) the pre-existing structure is not reactivated.

Structural inheritance, as considered in this article and as described above, is one of many causes for individual fault segments to be systematically misoriented relative to the overall trend of a fault with a consistent sense of stepping in map view. These include upward propagation of an older fault, fault nucleation above a deeper structure and rotation of the stress field either in space or in time (Mandl, 1987; Treagus and Lisle, 1997; Jackson and Rotevatn, 2013; Freitag et al., 2017; Morley, 2017; Worthington and Walsh, 2017; Collanega et al., 2019; Deng and McClay, 2019). In this paper we consider only the case of fault growth under the influence of an older and deeper structure but we have included at least one fault zone from the Columbus Basin where it is believed that there has been a temporal change in stress direction during fault growth (Freitag et al., 2017), with the resulting fault geometry being similar to faults formed under the influence of a pre-existing structure.

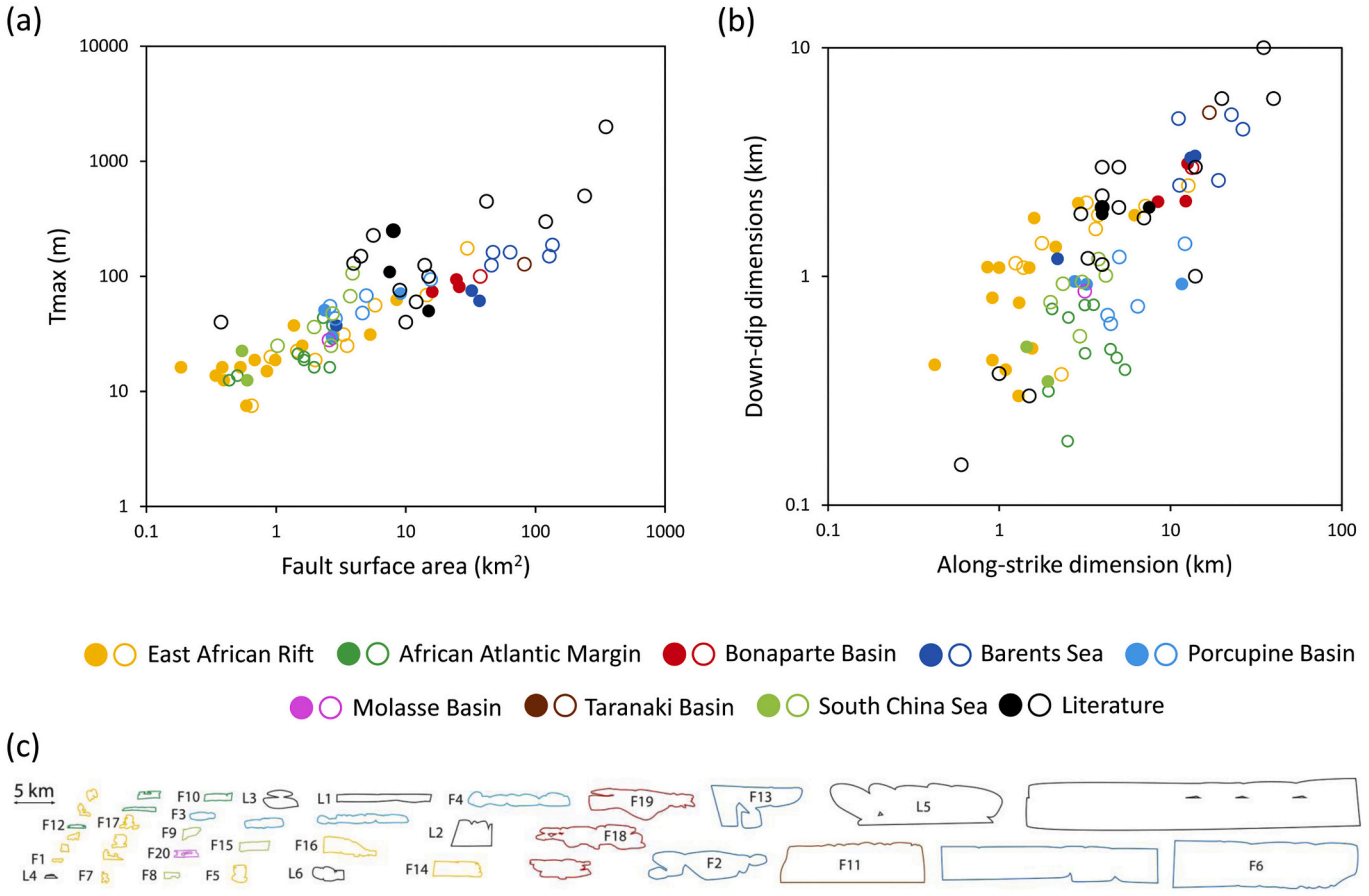

Fig. 5. (a) Relationship between maximum throw (*Tmax*) and fault surface area. (b) Down-dip dimension (*H* in Table 1) versus along-strike dimension (*L* in Table 1). (a) and (b) Full and empty symbols represent complete and incomplete faults, respectively. (c) Outlines of 39 studied fault zones shown at a similar scale with increasing fault surface area from left to right. The labels are the same as in Figs. 1 and 6.

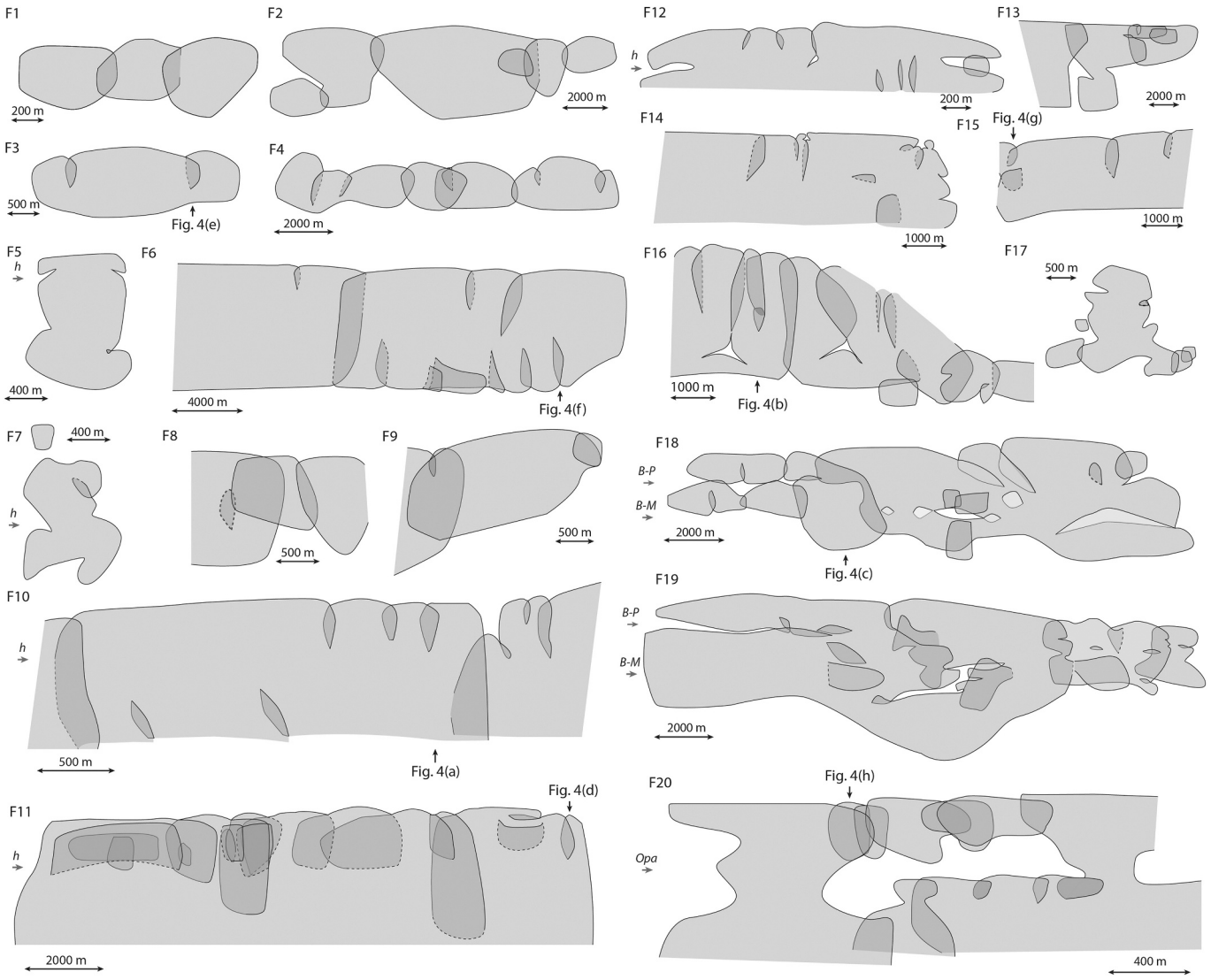

Fig. 6. Examples of studied fault zones. F1-11: Faults that present relatively simple relay distributions. F12-F20: Complex faults that display various combinations of the different types of relay. F1, F5, F7, F14, F16, F17: East African Rift; F2, F6, F13: Barents Sea; F3, F4: Porcupine Basin; F8, F9, F15: South China Sea; F10, F12: African Atlantic Margin; F11: Taranaki Basin; F18, F19: Bonaparte Basin; F20: Molasse Basin. All the faults are shown on strike projections at an approximate 1:1 vertical to horizontal scale. Thin black lines represent tip-lines and dotted lines represent branch-lines. Locations of the sections shown in Fig. 4 are indicated. The small grey arrows indicate the approximate levels of specific horizons influencing segmentation and discussed in the manuscript.

The second geological control considered is referred to as the mechanical heterogeneity (Table 1, *M.H.*), representing the degree of mechanical contrast within the faulted sequence at the scale of fault mapping. Mechanical heterogeneity is known to be a key controlling factor on the growth and geometry of extensional faulting based on studies of faults in two (e.g. Muraoka and Kamata, 1983; Peacock and Sanderson, 1992; Childs et al., 1996a; Ferrill and Morris, 2003; Schöpfer et al., 2006; Roche et al., 2012; Ferrill et al., 2017) and three dimensions (Mansfield and Cartwright, 1996; Nicol et al., 1996; Tvedt et al., 2013; Wilson et al., 2013; Lăpădat et al., 2017). Whilst objectively assessing this control at the time of faulting can be challenging, we nevertheless expect different degrees of mechanical heterogeneity among the studied areas and this control is deemed important (i.e. *M.H.* assigned a value of 1 in Table 1) for two of the studied areas. In the Molasse Basin, the faulted Mesozoic section contains a thick (120 m) clay dominated unit, the Opalinus Clay, over- and underlain by more competent limestone units, that provides a strong mechanical heterogeneity (Roche et al., 2020). In the Bonaparte Basin, two weaker stratigraphic units within the calcarenite/mudstone dominated sequence, at the Base Pliocene and the Base Miocene, are identified from well logs as zones of decreased P-wave velocity. The Base Pliocene in this area is an unconformity at which some faults terminate but in our study we include only faults formed significantly later than the unconformity which have the same displacements above and below this unconformity. In the other datasets, the faulted sequences consist mainly of alternations of mudstones, sandstones and shales at shallow depth and we expect a more moderate to weak mechanical heterogeneity (i.e. *M.H.* assigned a value of 0 in Table 1).

The third aspect of the geological setting identified in Table 1 is whether or not the faults are stratabound (Table 1, *S.B.*), referring to faults that are confined to a particular sedimentary unit so that they often have high fault surface aspect ratios (Nicol et al., 1996; Soliva et al., 2005; Roche et al., 2013; Ghalayini et al., 2017). The faults studied in the Porcupine Basin are post-rift, stratabound faults confined to a c. 1 km thick sequence of Paleocene and Eocene strata. Some of the smallest faults studied in the East African Rift (i.e. 5 faults) are also stratabound and restricted to a vertical interval of c. 400 m; the remaining 18 larger faults from that dataset are either blind faults or reach the sea-floor and have variable down-dip dimensions.

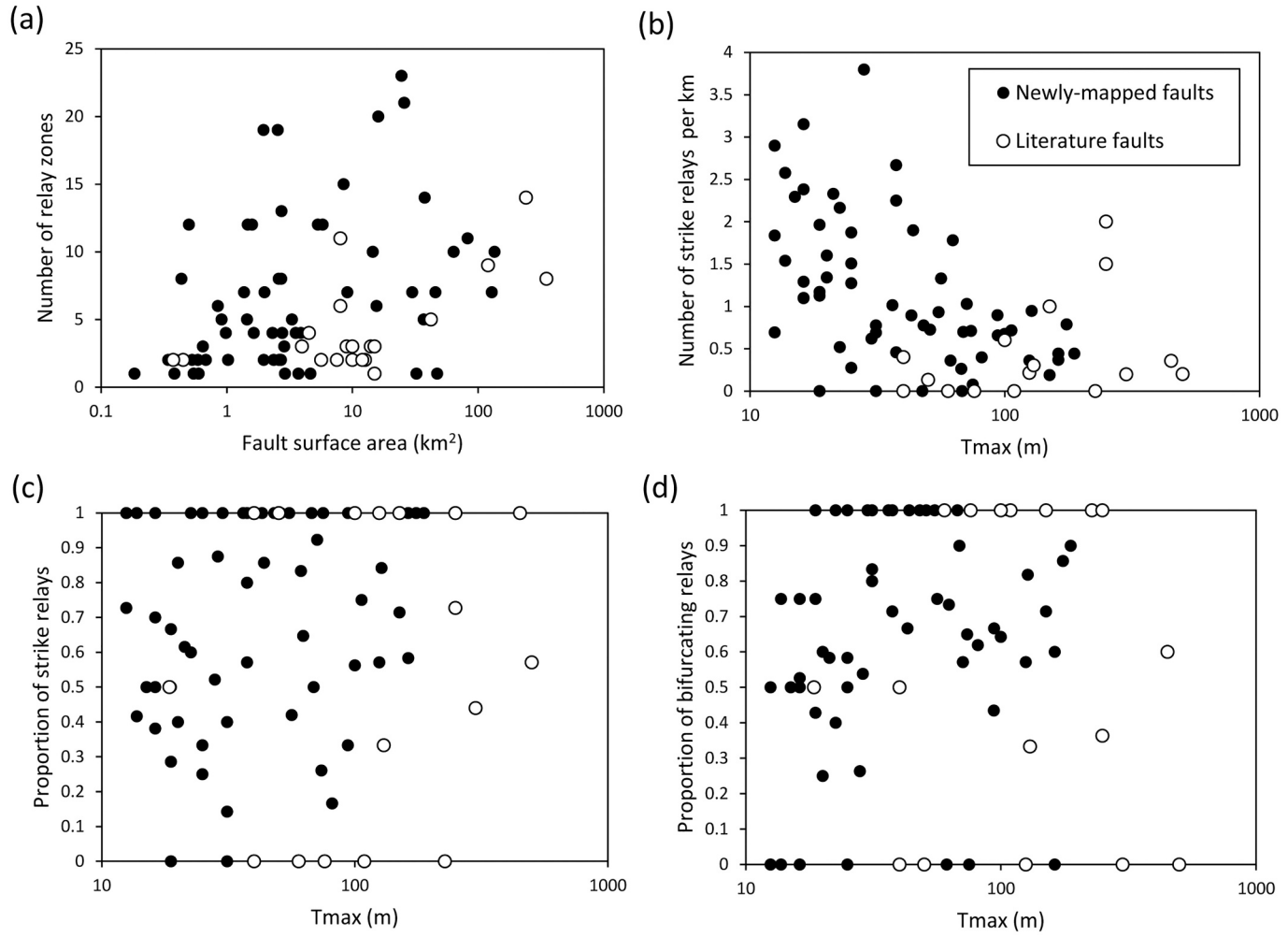

Fig. 7. (a) Plot of the number of relay zones against fault surface area. (b) Plot of the number of strike relay zones per kilometre of mapped fault trace versus the maximum throw along the fault trace (*Tmax*). (c) Plot of the proportion of strike relay zones against the maximum throw. (d) Plot of the proportion of bifurcating relay zones against the maximum throw. (a-d) Legend as in (b).

Quantitative expressions of the degree of inheritance, based for example on the obliquity between newly-formed faults and the reactivated faults (Corti, 2008; Clifton et al., 2000; Worthington and Walsh, 2017), and of the mechanical heterogeneity (Ferrill et al., 2017; Roche et al., 2020) are possible but these are beyond the scope of this paper which aims to assess first-order controls on fault growth by examining end-member cases and general trends. In Table 1 we identify the areas where these controls are clear but we recognise that the same controls may exist in the other areas and have a more subtle impact or may be subject to other controls not considered here. The controls identified for the faults taken from the literature are derived from the relevant publications and given in Table 1. Selected relevant information on the geological settings of these faults are provided, where appropriate, in the results section.

4. Mapping and sampling effects from seismic data

Here we discuss the biases in comparing fault geometries that may arise from fault mapping from different areas, using data of various qualities, and from comparing faults with different size and shape. Despite these biases, there are trends in our data and correlations with geological settings, which become apparent when individual datasets are compared, as discussed in Sections 5 and 6.

4.1. Resolution effects on categorisation of individual relay zones

3D seismic reflection data are the best source of 3D maps of fault surfaces, however there are clear limitations on what can be imaged. The lower limit of seismically resolvable fault throws means that the tip regions of faults are not imaged so that fault surfaces extend further than they can be mapped seismically (Badley et al., 1990; Watterson et al., 1996; Rotevatn and Fossen, 2011). While this means that the overlap areas on relay zones are larger than those mapped here, this will not affect the mapped form of the relay zones and is very unlikely to cause a dip relay zone to be mapped as a strike relay zone. We do not therefore consider that limitations of throw resolution will impact on our geometrical classification of resolvable relay zones.

A more significant effect for the purposes of this study is the lateral resolution of the data. To discuss imaging of relay zones we define the lateral resolution as the distance between two fault surfaces below which they appear as a single fault on a seismic line. Relay zones with separations that are lower than this limit will not be identified and are not of concern here. However, we cannot rule out the possibility that relay zones below the limit of resolution are systematically different to those that are imaged, and observations must be recognised as applying only to the scale at which they are made.

Of more concern is the possibility that cylindrical relay zones, in

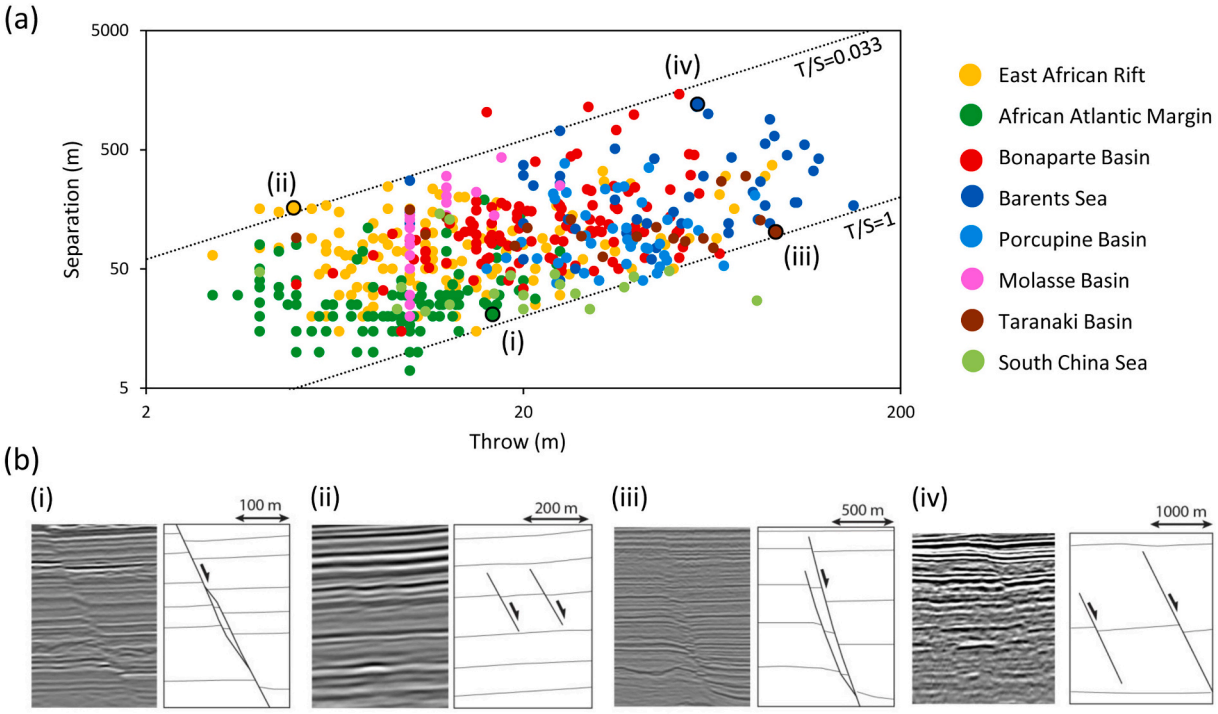

Fig. 8. (a) Plot of the separation versus throw across the relay zones for different datasets. Two lines of constant throw to separation ratio (*T/S*) are shown. (b) Examples of sections through relay zones at high (i and iii) and low (ii and iv) throw to separation ratios. The corresponding relay zones are indicated in (a). Each section is presented with an approximately 1:1 vertical to horizontal scale.

which the separation between the bounding faults varies and is locally lower than the lateral resolution, may appear to have a bifurcating form. Therefore, we may expect that resolution limits may bias our classification of relay zones in favour of bifurcating geometries. Lateral resolution is unlikely to cause a dip relay zone to be mistaken for a strike relay zone or vice versa.

A third source of bias is the large degree of subjectivity in interpreting dip relay zones as opposed to strike relay zones from 3D seismic volumes. The interpretation of dip relay zones and particularly those that are breached can be highly subjective particularly when the separations are low and/or there is little overlap between the fault segments. This is primarily because dip relay zones are generally in the plane of bedding so that horizon slices or horizon maps do not provide a second interpretable cut through the relay zones and the interpretation is based on vertical profiles only. In the case of strike relay zones, seismic profiles and horizon slices provide a better basis for identifying and objectively mapping them. This effect is likely to introduce a bias towards the recognition of strike over dip relay zones.

4.2. *Scale and data resolution effects on fault surface parameterisation*

We do not expect that seismic resolution will significantly impact the assignment of individual relay zones to a particular category, but there are potential sources of bias in deriving the relative proportions of these categories on individual faults, particularly as our sampling covers a range of different fault sizes (Fig. 5). Large faults, with large surface areas, would be expected to have greater numbers of relay zones than small faults but this is not the case for the database as a whole (Fig. 7a). This counterintuitive result arises from a systematic decrease in the measured frequency of relay zones as the throw on the fault surface increases (Fig. 7b) to give an *effective* decrease in lateral resolution for larger faults. For the studied data, when the summed throw on two relay bounding faults as seen on a seismic line is equal to the fault separation, two faults are rarely resolved, even for the highest quality 3D seismic datasets. This observation is reflected in Fig. 8 by the lower boundary of the data defined by a throw to separation ratio of 1. We note that this limiting ratio is for the separation measured in the centre of the relay zones in 3D (i.e. at the relay axis, see Camanni et al., 2019 for further details). Smaller separations can be observed on individual seismic lines and higher ratios are expected in this case. This observation is considered to be due to increased distortion of the seismic signal associated with larger offset faults and to increased strain within relay zones at higher throws leading to increased difficulty in imaging. Therefore, as fault surface area and fault throw increase, the minimum separation at which relay zones can be recognised also increases so that the number of resolved relay zones does not increase with fault surface area. While this trend is key for understanding sampling effects on relay zone mapping from seismic data, it does not necessarily impact on either the proportion of strike relay zones or their orientations, which are the two aspects of most concern in this paper (Fig. 7 c and d).

4.3. *Fault aspect ratios*

While the sizes of the faults do not impact on segment parameterisation, the proportion of strike versus dip relay zones may be dependent on the shapes of fault surfaces, with higher mapped aspect ratio fault surfaces promoting the sampling of strike relay zones (Fig. 9a). The proportion of strike relay zones is larger both for larger faults that extend below the lower edges of the seismic volume, so that they have artificially high mapped aspect ratios within the seismic volume (incomplete faults in Fig. 9 a and b) and for stratabound fault surfaces (Fig. 9 a and b). Non-stratabound "complete" faults do not show a relationship between the proportion of strike relay zones and aspect ratio, suggesting that the trend observed for incomplete faults is due to data aliasing rather than reflecting a real trend in non-stratabound faults.

A tendency to underestimate the numbers of cylindrical relay zones could be expected as we do not include relay zones that extend outside the mapped fault surface in our categorisation by relay zone form, and a cylindrical relay, by definition, is longer than a bifurcating one at the same position on the fault. However, Fig. 9c shows no relationship

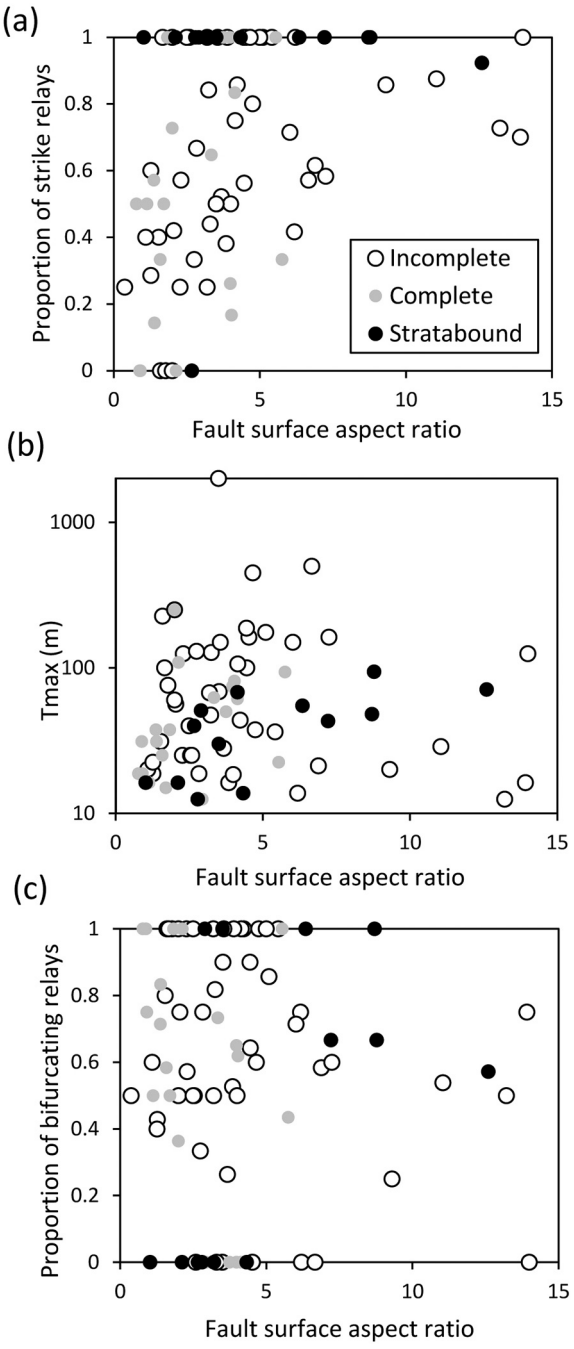

Fig. 9. Impacts of fault surface aspect ratio on the segmentation. Plots of (a) the proportion of strike relay zones, (b) the maximum throw, and (c) the proportion of bifurcating relays, vs. the fault surface aspect ratio. (a-c) Legend as in (a). Data include newly-mapped faults and literature faults.

between the relative numbers of bifurcating versus cylindrical relay zones as a function of aspect ratio, suggesting that incomplete sampling has a negligible effect on the database.

5. The 3D geometries of segmented normal faults

Inspection of the selected faults illustrated in Figs. 1 and 6 provides a visual impression of the broad range of fault surface geometries that have been mapped previously and in this study. This selection includes faults with the following attributes: (i) large central areas with no segmentation and relay zones restricted to bifurcation at the outer boundaries of the fault surface (e.g. Fig. 6, F6 and F12) and particularly towards the contemporaneous free surface (e.g. Fig. 1, L2 and Fig. 6, F3), (ii) multiple relay zones transecting the entire fault surface (e.g. Fig. 1, L1 and Fig. 6, F1 and F2), (iii) multiple relay zones that are remote from the fault tip (e.g. Fig. 6, F19) and (iv) "holes" in the centre of the fault surface (e.g. Fig. 6, F18-20). Although this complexity and variability could be described in many different ways, we consider that characterisation in terms of relay zone form and orientation is an approach that is both objective and readily applied to a wide range of geometries. Our approach is to represent the geometry of fault surfaces by cross-plotting the proportion of relay zones on the fault that are bifurcating as opposed to cylindrical, against the proportion that are strike as opposed to dip (Fig. 3). The plot for the newly-mapped and literature faults (Table 1) is shown in Fig. 10, categorised further by dataset (colours) and number of relay zones on the fault (circle size).

5.1. Fault segmentation data derived from the literature

This section provides an outline of the published fault surfaces that have been parameterised as described previously and incorporated into this study. Although relay zone form and orientation have not been used explicitly in the literature, these papers have described and/or illustrated these geometrical attributes for particular faults and some have related them to underlying geological controls.

Of the 24 faults taken from the literature, 13 lie at the corners of the plot in Fig. 10 and six at the edges of the plot. The majority of individual faults therefore contain either one or two relay zone types. While it is likely that higher resolution data would allow identification of a more varied range of relay zone types on these faults (see below), those mapped are presumably the largest segments in the fault array and reflect controls acting at the largest scales. Hence, these faults demonstrate that, at the largest scale, the dominant relay zones on particular faults may be all of one type giving rise to relatively simple geometries. Two end-member geometries observed in the literature are faults that contain only cylindrical strike relay zones (lower right-hand corner of Fig. 10) and faults that contain only bifurcating strike relay zones (upper right-hand corner of Fig. 10). These fault geometries are illustrated by published examples from the Levant Basin (Fig. 1, L1) (Baudon and Cartwright, 2008) and the Taranaki Basin (Fig. 1, L2) (Collanega et al., 2019). It is worth noting that these two fault geometries are commonly recognised or inferred in the broader literature. They have been inferred for natural faults mapped in 2D (e.g. Segall and Pollard, 1980; Trudgill and Cartwright, 1994; Soliva et al., 2006) and 3D seismic data (e.g. Childs et al., 1995; Walsh et al., 1999; Baudon and Cartwright, 2008; Collanega et al., 2019; Giba et al., 2012; Worthington and Walsh, 2017; Marchal et al., 2003), generated in sandbox experiments (e.g. Ackermann et al., 2001) and numerical models (e.g. Schöpfer et al., 2016) and incorporated into a range of modelling exercises (e.g. Willemse, 1997; Crider and Pollard, 1998; Soliva et al., 2008; Manzocchi et al., 2008; Islam and Manzocchi, 2019; Oglesby, 2020).

The upper left-hand corner of the plot is occupied by faults containing only bifurcating dip relay zones (Fig. 10). Fig. 1(L3) provides a representative example of a fault from the Egersund Basin, Norwegian North Sea (Tvedt et al., 2013). This fault is restricted to a thick cover sequence of mudstone with upper and lower segments separated by two bifurcating dip relay zones that are aligned horizontally in the organic shale of the Tau Formation (Fig. 1, L3, level *Sh*). By contrast, accounts of faults containing only cylindrical dip relay zones (lower left-hand corner in Fig. 10) are sparse in the literature. The fault shown in Fig. 1(L4) is from a polygonal fault system in the Bathurst Island Group regional seal, Petrel Sub-basin, offshore NW Australia and is composed of three segments separated vertically by an unbreached relay zone and a breached relay zone at greater depths (Seebeck et al., 2015). In this case, however, the dip linkages are not related to the presence of incompetent layers in the faulted sequence but rather result from initially unconnected faults that formed in different tiers of the polygonal fault system that became kinematically related (see also Laurent et al., 2012).

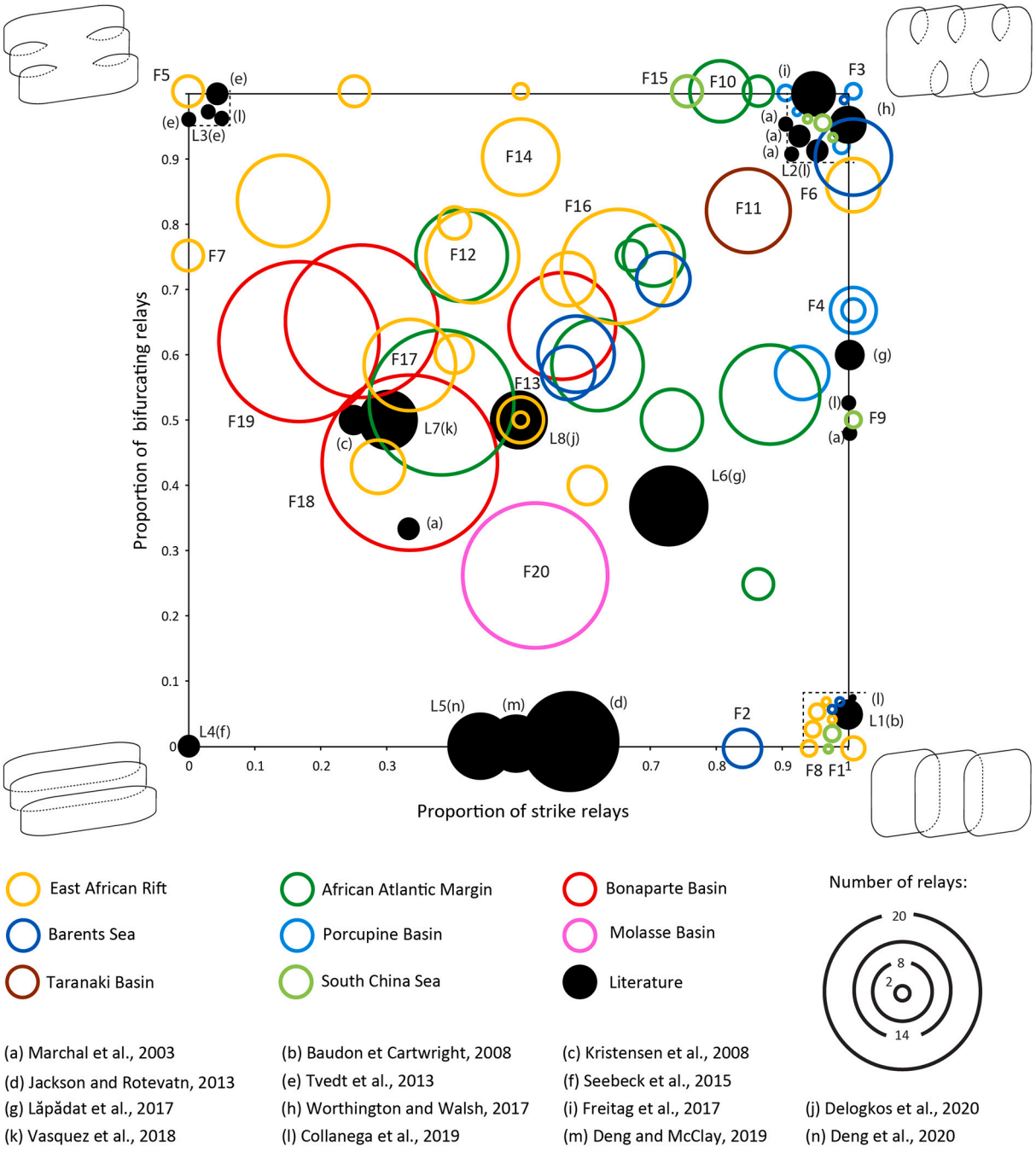

Fig. 10. Proportion of bifurcating relays vs. proportion of strike relays for 61 newly mapped normal fault zones in 8 different datasets and 24 normal fault zones from the literature. Faults L1-L8 and F1-F20 are illustrated in Figs. 1 and 6, respectively. The dashed squares in three of the four corners contain a number of faults that should plot exactly in the corner but are shown in this way to make them visible.

Although many of the literature faults are simple and plot at the corners of Fig. 10, some are more complex. A model of fault surface geometry proposed in the literature is a patchwork of distinct segments separated by a combination of cylindrical dip and strike relay zones (Mansfield and Cartwright, 1996; Willemse and Pollard, 2000; Kattenhorn and Pollard, 2001; Peacock, 2002); such faults would plot on the lower horizontal axis in Fig. 10. This pattern has been observed from detailed mapping. For example, Jackson and Rotevatn (2013) (Fig. 10, point *(d)*) described a fault zone from the Suez Rift that is composed of four, amalgamated fault segments that offsets a pre-rift crystalline basement below a salt-bearing interval of Late Miocene and six fault segments in the Pliocene cover strata above the salt. The supra- and sub-salt segments are interpreted as soft-linked by six cylindrical dip relay zones and interact laterally through eight breached and unbreached cylindrical strike relay zones, which are all but one right-stepping. Very similar geometries from the Enderby Terrace, NW Australia are described in Deng and McClay (2019) (Fig. 10, point *(m)*) and Deng et al. (2020) (Figs. 1 and 10, L5). In this case, a series of cylindrical dip relay zones at a mechanically incompetent Lower Triassic Locker Shale (Fig. 1, L5, level *Sh*) separate a reactivated pre-existing fault below the shale, from en-echelon segments separated by cylindrical strike relay zones within the more competent Triassic units above.

A similar, but rather more complicated fault has recently been described from the Inner Moray Firth Basin, offshore Scotland (Lăpădat et al., 2017) (Fig. 1, L6). Like the fault zones from the Suez Rift and the Enderby Terrace, this fault zone contains cylindrical dip relay zones that

are associated with a mechanically incompetent Lower–Middle Jurassic pre-rift interval and several fault segments separated by cylindrical strike relay zones above the dip relay zones. Additionally, the fault also contains a series of bifurcating strike relay zones that tend to be rooted vertically in the incompetent interval (Fig. 1, L6, level *Cl*), resulting in a fault which plots towards the centre of Fig. 10. Other complex segmented faults have also been previously described from analogue models and outcrop data. Fig. 1(L7) shows an example from an analogue model by Vasquez et al. (2018) (Fig. 10, L7), with cylindrical dip and strike relay zones that are associated with ductile silicone layers with a similar fault zone configuration to those described above, but also with bifurcating dip relay zones that are aligned in the incompetent layers (Fig. 1, L7, level *Si*). Finally, Fig. 1(L8) shows a fault zone mapped in three dimensions using successive mapping of mine faces in an opencast lignite mine in Greece by Delogkos et al. (2020) (Fig. 10, L8). The fault contains four strike relay zones and four dip relay zones that have either a cylindrical or bifurcating form and, in a similar manner to the previous examples described, the influence of a thick mechanically weak unit (in this case a lignite unit) is believed to control the location of the 3D segmentation (Fig. 1, L8, level *Li*).

5.2. Fault segmentation data derived from newly-mapped faults

A wide diversity of fault surface geometries is recognised among the newly-mapped fault zones that occupy most of the area of the plot in Fig. 10. We identify several faults with relatively simple geometries that plot at the corners of the plot in Fig. 10. Among these, faults with exclusively cylindrical strike relay zones or bifurcating strike relay zones are relatively common (i.e. lower and upper right-hand corners in Fig. 10), whereas faults that contain only bifurcating dip relay zones (i.e. that plot at the upper left-hand corner in Fig. 10), are less well represented and faults containing only cylindrical dip relay zones were not identified (i.e. lower left-hand corner in Fig. 10). Usually, however, the mapped faults display more complex geometries with different proportions of relay forms and orientations and hence do not plot on the edges or corners of Fig. 10. The rationale for this variability in fault geometry is discussed in detail in later sections.

5.3. Fault segmentation – general trends

A number of conclusions can be drawn from the distribution of the datapoints representing all the investigated faults, both newly-mapped and from the literature (Fig. 10). Data plot in virtually all areas of the plot so that all of the various geometries illustrated in Fig. 3 can be found in nature. The data are not evenly distributed over the plot but there are clusters at the corners and towards the centre of the plot. The datapoints located at the corners of the plot are usually, but not exclusively, derived from faults where few relay zones have been mapped and we interpret

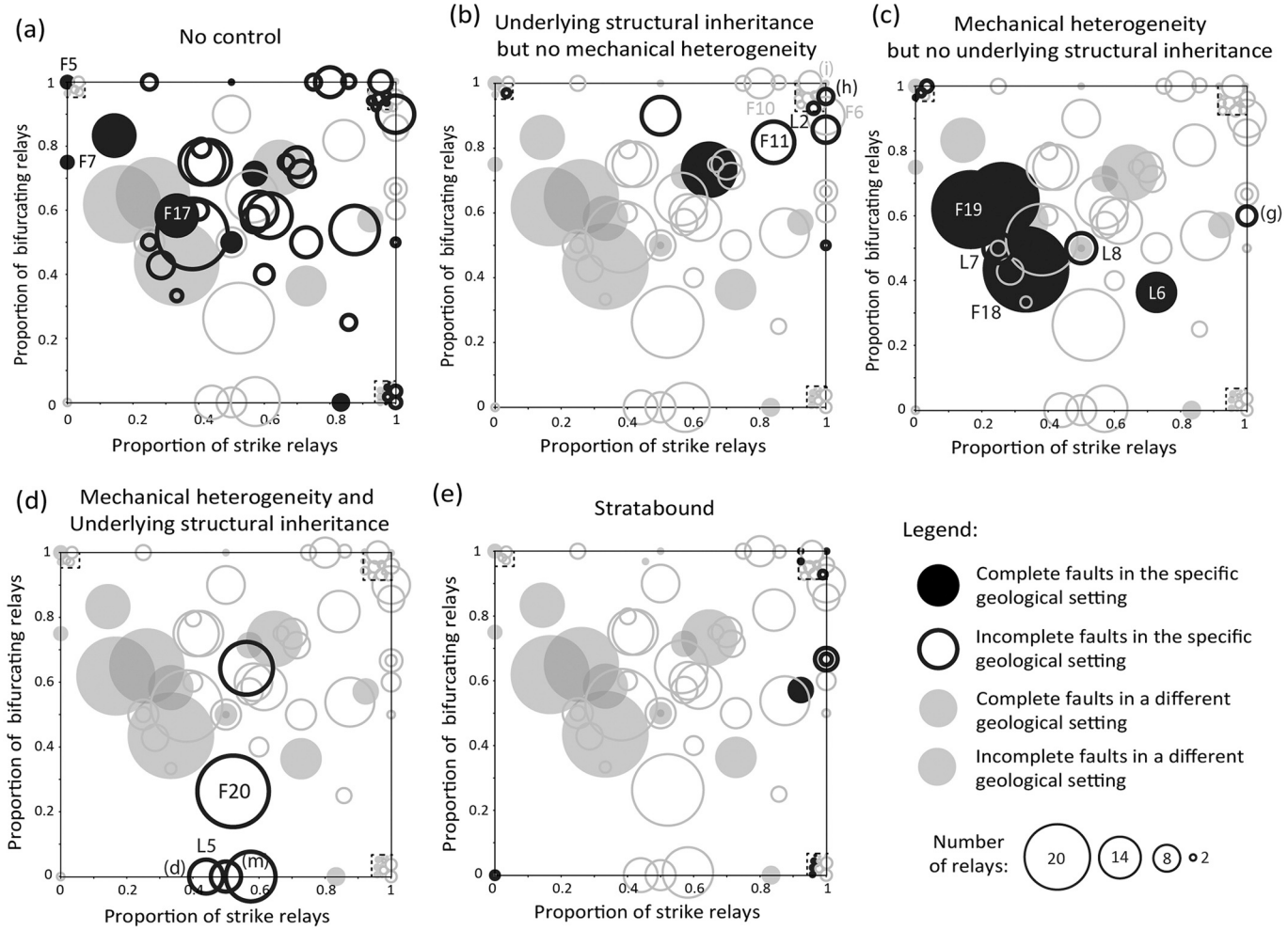

Fig. 11. Proportion of bifurcating relays vs. proportion of strike relays for the 8 different datasets and the literature examples showing the geological controls. (a) Faults in black show an absence of strong geological controls. (b-e) Faults in black show influence of an underlying structural inheritance (b), of mechanical heterogeneity (c), a combined effect of mechanical heterogeneity and underlying structural inheritance (d), or are stratabound (e). The plotted circles for individual faults are scaled as a function of the number of relay zones. Empty and full circles represent complete and incomplete faults.

their locations on the plot as an artefact of small sample sizes. When the number of relay zones that can be mapped is greater than 8 to 10, the datapoints do not lie on the plot axes leading to the key conclusion that, when sufficient resolution is available, faults comprise segments that are separated by bifurcating and cylindrical relay zones in both strike and dip orientations.

Faults with greater numbers of mapped relay zones tend to lie in the upper half of Fig. 10 so that, in general, individual faults have a predominance of bifurcating over cylindrical relay zones. There is no similar trend in terms of the frequency of strike as opposed to dip relay zones and all ratios between these are equally well represented. Faults from a single area also show a wide variety of three-dimensional geometry as illustrated by the largest dataset, i.e. the East African Rift, in which the 23 faults occupy most of the plot area. This particular dataset can be subdivided into different subsets that plot in different parts of Fig. 10 for reasons of different geological setting discussed below. While the data in Fig. 10 are distributed widely over the plot, there are some trends that reflect underlying controls on fault surface geometry. In the following sections we examine in detail aspects of the data in Fig. 10 and individual faults, in an attempt to provide a generalised description of the controlling factors on the segmentation characteristics of normal faults.

6. Geological controls on 3D fault surface geometry

The previous section described and charted the wide variety of 3D fault surface geometries that have been described in the literature and identified in this study (Fig. 10). While some aspects of the data distribution reflect data limitations (see Section 4), a significant component of variability is attributed to underlying geological controls on the form and orientation of relay zones, which will be described in this section. In common with many previous studies, we consider the two most significant controls to be the mechanical heterogeneity of the faulted sequence and the influence of pre-existing structure (e.g. Giba et al., 2012; Jackson and Rotevatn, 2013; Morley, 2017; Lăpădat et al., 2017; Worthington and Walsh, 2017; Collanega et al., 2019; Deng and McClay, 2019). The approach taken is to examine sub-sets of the data in which different combinations of controls are expected to be important (Fig. 11). These controls are categorised on a fault-by-fault basis (Table 1) using the criteria described in Section 3.2.

6.1. Fault geometry under homogeneous conditions

For many of our datasets there is no reason to expect that there was either a strong mechanical heterogeneity of the faulted sequence at the scale at which the faults are mapped, or clear evidence for an inherited structural control on segmentation; these faults are highlighted in Fig. 11a. While we treat these faults as having formed in a broadly homogeneous sequence under a uniform stress field, we recognise that there may be sub-resolution mechanical heterogeneities or other unrecognised controls on fault geometry. Despite these caveats, it is useful to examine the distribution of these data in relation to those where strong controls are evident.

The datapoints for faults with no apparent control, particularly with a larger number of relay zones, tend to lie towards the centre of the cross-plot with a tendency towards higher proportions of bifurcating relay zones (Fig. 11a). The proportion of strike relay zones covers the full range of possible values but the faults with the highest numbers of relay zones are concentrated in the upper central part of the graph and those with fewer mapped relay zones lie at the boundaries of the graph. Some faults mapped in the East African Rift dataset occupy the space in the upper left corner of Fig. 10 with large proportions of dip relay zones (e.g. Figs. 6 and 11a, F5, F7 and F17). These faults have low aspect ratios and a near-circular shape, circumstances that promote the occurrence of dip relay zones as described in Section 4.3. We conclude that, in the absence of strong geological controls on faulting, faults display a wide range of segmentation patterns and all combinations of form and orientation is the norm.

6.2. Influence of underlying structure

Faults formed under the influence of underlying structures in relatively homogeneous cover sequences lie in the upper right area of Figs. 10 and 11b, i.e. they display high proportions of strike and bifurcating relay zones. These relay zones are associated with vertical twisting of the fault surface above the reactivated structure, often resulting from a component of oblique extension. For example, Neogene reactivation of pre-existing Cretaceous normal faults in the Taranaki Basin is accompanied by upward clockwise twisting of fault segments with the formation of numerous left-stepping bifurcating relay zones (e.g. Figs. 6 and 11b, F11 or Figs. 1 and 11b, L2) (Collanega et al., 2019; Giba et al., 2012). Worthington and Walsh (2017) describe similar right-stepping segment geometries arising from oblique Eocene reactivation, with a c. 5° obliquity from pure orthogonal, of pre-existing Jurassic faults in the Porcupine Basin (e.g. Fig. 11b, point *(h)*). For these examples the points at which the fault surface bifurcates into two relay-bounding segments are at a similar level on the parent fault surface, a level that is not necessarily directly at the top of the pre-existing structure (e.g. level *h* in Fig. 1, L2 and Fig. 6, F11).

Although we focus in this paper on the control of pre-existing structure, we consider this to be a subset of cases in which extension direction is oblique to the overall trend of a fault. For example, Freitag et al. (2017) describe a situation in which a temporal change in extension direction caused the formation of a fault surface comprised of bifurcating and right-stepping strike relay zones, and that plots at the upper right-hand corner of Fig. 10 (Fig. 11b, point *(i)*). Mandl (1987) described how similar geometries arise when faults propagate through a heterogeneous stress field. Arrays of en-echelon faults may also form where mechanical layering is inclined, rather than perpendicular to, the propagation direction of fault surfaces (Mandl, 2005; Schöpfer et al., 2007). The impact of these processes is generally more apparent at the upper tip-lines of faults but may occur anywhere around the fault tip-line. For example, the upper tip-line of fault F6 from the Barents Sea dataset shows three right-stepping bifurcating relay zones but the lower part of the fault is also segmented with five left-stepping bifurcating strike relay zones. Similarly, the fault F10 from the African Atlantic Margin shows five left-stepping bifurcating strike relay zones on the upper tip and two at the lower tip (Figs. 6 and 11a).

6.3. Influence of mechanical heterogeneity

Vertical segmentation and the formation of dip relay zones is often related to strong mechanical heterogeneity (Peacock and Xing, 1994; Childs et al., 1996a; Rykkelid and Fossen, 2002; Koledoye et al., 2003; Walsh et al., 2003; Schöpfer et al., 2006; Ferrill et al., 2017). This is reflected in the generally low proportions of strike relay zones for faults in the presence of strong mechanical heterogeneity as is evident for the faults mapped in the Bonaparte Basin (e.g. Fig. 11c, F18 and F19). Here two relatively weak stratigraphic levels are identified within the faulted sequence, at the Base Pliocene and Base Miocene. Although there is evidence of fault reactivation in this area, three of the faults mapped are not considered to have been influenced by underlying structures and are readily distinguished from nearby faults that form above earlier Mesozoic faults (Saqab and Bourget, 2015). Two examples are illustrated in Fig. 6 (F18 and F19) and both faults show numerous dip relay zones that are aligned along the Base Pliocene (Fig. 6, level B-P) and to a lesser extent the Base Miocene incompetent layer (Fig. 6, level B-M).

An apparent exception to the increase in dip segmentation due to mechanical heterogeneity from the literature is the data we have derived from Lăpădat et al. (2017), where, for one of their faults, we have measured only strike relay zones (Fig. 11c, point *(g)*). However, in that paper the authors emphasise the significance of layering in promoting

vertical segmentation. The reason for this apparent contradiction is that the dip relay zones on these faults are now observed as layer parallel bends in the faults which we have not measured as dip relay zones. Therefore, the datapoints derived from Lăpădat et al. (2017) could indicate a much lower proportion of strike relay zones than is represented in Fig. 11c (L6 and point *(g)*). Delogkos et al. (2020) describe a similar fault in which a long, initially underlapping dip relay is only identifiable as a lower-dip strike-parallel panel on the fault surface (Fig. 11c, L8).

The presence of mechanical heterogeneity may not only result in greater numbers of dip relay zones but may also limit the vertical extent of strike relay zones. For example, the left-hand side of F18 in Fig. 6 is divided into two portions, above and below the Base Pliocene horizon, that are separated by dip relay zones centred on this horizon. A series of strike relay zones separate the segments above and below but these relay zones terminate at the Base Pliocene and are not aligned across it. Similar patchworks of segments have been described in the Gulf of Mexico (Mansfield and Cartwright, 1996) and in the Wessex Basin, UK (Kattenhorn and Pollard, 2001) with dip segmentation at the level of relatively incompetent formations and unaligned strike segments above and below. Similar patterns of vertically restricted strike relay zones have been produced in analogue models of extensional faulting in the presence of weak layers (Fig. 1, L7, levels *Si* and Figs. 10 and 11d, L7) (Vasquez et al., 2018).

There may also be a tendency for the locations of bifurcation points, where single fault surfaces split into two segments in bifurcating strike relay zones, to be controlled by mechanical heterogeneity of the sequence. For example, bifurcation points in F18 in the Bonaparte Basin (Fig. 6) are preferentially located at the Base Pliocene horizon. There are also many more examples of fault bifurcation occurring within a restricted depth range on individual faults which we suspect are defined by a marked mechanical heterogeneity (e.g. Fig. 6, level *h* in F10 and F12) but for which we do not yet have corroborating evidence.

Our analysis of faults in sequences with strong mechanical contrasts, such as those within the Bonaparte Basin, show the full spectrum of impacts of sequence control on segmentation and on the elevations of fault tips. This spectrum of structure can also be recognised in a fault from the Inner Moray Firth Basin, offshore Scotland described by Lăpădat et al. (2017) (Figs. 1, 10 and 11c, L6) where a mechanically less competent unit within the Lower-Middle Jurassic pre-rift interval (Fig. 1, L6, level *Cl*) is potentially associated with (i) alignment of dip relay zones, (ii) cylindrical strike relay zones above the cylindrical dip relay zones and (iii) bifurcating strike relay zones rooted vertically in the same interval as the cylindrical dip relay zones.

6.4. Combined influences of mechanical heterogeneity and underlying structures

The fault studied in the Molasse Basin presents a moderate proportion of strike relay zones despite the strong mechanical heterogeneity in this dataset, and a low proportion of bifurcating relay zones despite the influence of an underlying structure (Fig. 10). This fault, illustrated in Fig. 6 as F20, shows a characteristic alignment of dip relay zones in the weak Opalinus Clay Formation (Fig. 6, level *Opa*), whereas above the clay the fault comprises left-stepping en-echelon segments bounded laterally by cylindrical relay zones. The vertical twist that occurs in a homogeneous sequence in response to the reactivation of a misoriented underlying structure, is interrupted here by the incompetent layer that decouples the lower portion of the fault that is directly connected to the pre-existing fault from its upper portion. The bifurcating relay zones found in the absence of a weak unit are replaced by cylindrical relay zones that are vertically restricted. Moderate proportions of strike relay zones are maintained as the increased proportion of strike relay zones due to reactivation is balanced by an increased number of dip relay zones due to the presence of the weak layer.

We propose that the pattern of segmentation observed in the fault from the Molasse Basin is the typical signature of the influence of pre-existing structures combined with a strong mechanical heterogeneity that creates favourable conditions for segments that are bounded both laterally and vertically by cylindrical relay zones. The sub-set of faults subject to both controls is shown in Fig. 11d. Previous studies by Jackson and Rotevatn (2013), Deng and McClay (2019) and Deng et al. (2020) display a similar structure (Figs. 1, 10 and 11d, points *(d)*, *(m)* and L5), in which there is an alignment of cylindrical dip relay zones along either a salt bearing or a thick shale dominated formation (Fig. 1, L5, level *Sh*) with en-echelon fault segments above.

6.5. Stratabound fault systems

Examples of stratabound faults have been mapped in two areas: the East African Rift and the Porcupine Basin. These faults lie on the right-hand side of Fig. 10 with high proportions of strike relay zones due to their limited dip dimensions and large aspect ratio that precludes the occurrence or the sampling of dip relay zones (Fig. 11e). In the East African Rift, stratabound faults have only cylindrical strike relay zones, whereas in the Porcupine Basin bifurcating relay zones dominate. Other potential examples not integrated in the database include sub- and supra-evaporite faults studied by Wilson et al. (2013) in the Halten Terrace on the mid-Norwegian continental margin, or segmentation observed on polygonal faults system by Ghalayini et al. (2017) in the Levant Basin.

6.6. Model linking fault geometry and geological controls

The discussions above and sub-samples of the dataset show that the 3D geometries of fault surfaces are dependent primarily on the heterogeneity of the faulted sequence and whether or not the fault segments are misoriented relative to the overall fault trend. To summarise schematically the general relationships identified in the previous sections, Fig. 12 shows the spectrum of fault surface geometries encountered and places them in a matrix defined by variation in these two controlling parameters. The figure illustrates how, in the absence of any strong

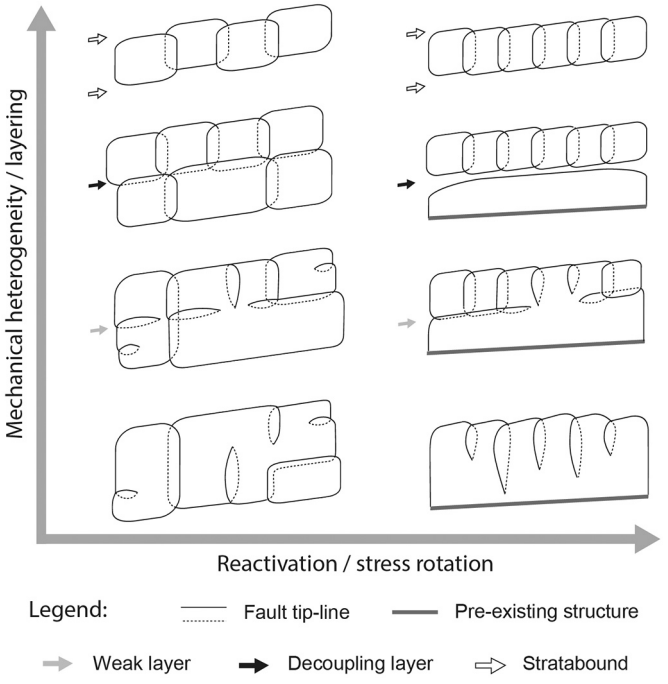

Fig. 12. Model linking segmented fault geometry to the presence/absence of an underlying structural control for a range of sequence heterogeneities, see text for details.

controls, all combinations of form and orientation are encountered (Fig. 11a). Increased impact of mechanical layering promotes the formation of dip relay zones (Fig. 11c), and in particular bifurcating dip relay zones centred on weaker units. As mechanical heterogeneity becomes more pronounced faults may comprise segments that are decoupled across weaker layers so that bifurcating relay zones are replaced with cylindrical relay zones to form a "patchwork" of initially unconnected fault segments. At the upper limit of this figure, we suggest that stratabound faults are end-member cases of layering control in which faults are contained within a single unit that limits their vertical extent giving rise to high fault aspect ratios and promoting the development of strike relay zones (Fig. 11e).

The two vertical columns in Fig. 12 illustrate the range of fault structure with and without the influence of an extension direction that is oblique to the overall structure. Of the many ways in which segment obliquity can arise, the figure illustrates the case of extension oblique to an underlying structure. The key difference with the introduction of the pre-existing structure is that the sense of stepping of the faults is consistent and the formation of strike relay zones is promoted (Fig. 11b). In the absence of mechanical heterogeneity these strike relay zones have a bifurcating form but become more frequently cylindrical when mechanical heterogeneity is introduced.

Segments that are misaligned relative to the overall fault trend are shown in Fig. 12 to arise from the presence of a pre-existing structure. However, other ways in which this geometrical relationship can develop have been previously identified. Spatial variations in the orientation of the principal stresses can cause bifurcation of a propagating fault surface and a systematic twisting of the fault segments (Mandl, 1987). To illustrate this case Fig. 12 could be modified to replace the line representing the pre-existing structure with a lower tip-line with segmentation characteristics reflecting a downward rotation of the stress field. Spatial variations in stress orientation are to be expected and dramatic vertical changes in stress orientations have been observed across salt layers (Roth and Fleckenstein, 2001; Tingay et al., 2011; Haghi et al., 2013).Temporal changes in stress orientation may also give rise to systematic stepping directions and Freitag et al. (2017) have described an example of segmentation formed in this manner.

7. Discussion

7.1. Effect of resolution on the characterisation of fault geometry

Normal faults are segmented over the full range of observable scales (Walsh and Watterson, 1990; Trudgill and Cartwright, 1994; Peacock and Sanderson, 1994; Willemse, 1997; Willemse and Pollard, 2000; Peacock, 2003; Long and Imber, 2011; Delogkos et al., 2020). In this study we have mapped relay zones with separations down to 20 m with the knowledge that there are scales of segmentation smaller than those we observe. To examine whether the nature of segmentation on these faults varies with the size of the relay zones, Fig. 13 shows changes in the average proportions of relay zone form and orientation for the faults within each of the 8 mapped datasets, as the lateral resolution is artificially degraded by excluding relay zones below a particular separation (indicated by datapoint labels in Fig. 13). With decreasing resolution and decreasing numbers of relay zones, datapoints representing each area, with the exception of the Bonaparte Basin, drift from the centre of the plot towards the margins. For most study areas the point moves downwards and to the right with decreasing lateral resolution, reflecting the fact that the largest relay zones in these datasets tend to be strike and cylindrical. Faults observed at low resolution therefore have a tendency to exhibit an apparent high proportion of strike relay zones, and faults observed at very low resolution may have an apparent high proportion of cylindrical strike relay zones (lower right-hand corner in Fig. 3). Therefore, while faults with only strike relay zones are frequently mapped from seismic data, it should be borne in mind that other unresolved relay forms are likely to be present.

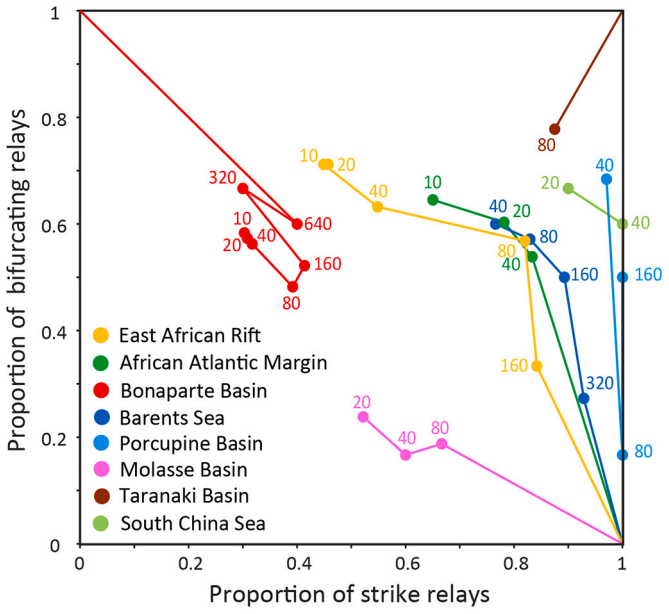

Fig. 13. Change in observed fault segmentation when all the relay zones with a size below a certain value are removed, which is equivalent to degrading the lateral resolution. Fault segmentation is calculated for decreasing lateral resolutions of 10, 20, 40, 80, 160, 320 and 640 m, as indicated by the numbering. For simplification, we use the data related to each entire dataset, rather than the individual faults.

It is tautological to say that more variability in fault surface structure occurs as more relay zones are mapped. Nevertheless, it is important to recognise that given a sufficient number of relay zones, all geometries of relay zone are likely to occur on all faults. It may be possible to distinguish different areas in terms of the frequency of segmentation and the dominant form or orientation of relay zones but there is no reason to expect that any particular setting has exclusively one type of relay zone. It is also worth noting that the mapping conducted here is at a single scale of observation and the individual mapped fault segments will themselves be segmented on smaller scales. Extrapolation of the trends in Fig. 13 to fault separations lower than those achieved in seismic imaging suggests that higher proportions of bifurcating and dip relay zones are likely to occur below the limit of seismic resolution.

7.2. Relating fault structure to geological controls

The assignment of particular geological parameters to a particular area can be subject to significant uncertainty. One of the most compelling lines of evidence for the conditions at the time of faulting is the geometry of the faults themselves. Faults that step across layering and the preferential location of fault segments in specific layers can be suggestive of mechanical heterogeneity (Childs et al., 1996b; Wilkins and Gross, 2002; Ferrill et al., 2017) and could be used as the basis for defining the relative competence of adjacent units. Similarly, en-echelon segments with a consistent sense of stepping can be taken as evidence for a structural inheritance control on fault initiation and propagation (Clifton et al., 2000; Ferrill et al., 2016). To objectively determine controls on 3D fault zone structure these criteria are not appropriate. Instead, to identify those cases where we consider there is a clear control, we rely on additional information on the mechanical stratigraphy, for example from direct measurement of rock properties, or evidence for the presence of pre-existing faults from mapping (see Section 3.2). There are however many situations in which fault geometry is suggestive of a systematic control but there is no additional information to support assignment of a particular controlling parameter. For example, fault F12 from the African Atlantic Margin dataset, has a number of bifurcation

points and two dip relay zones about halfway up the mapped fault surface (level *h* in Fig. 6) which may suggest some sequence control on fault geometry but we do not have any evidence from the character of the sequence to make this assignment. The point representing fault F12 in Fig. 10, together with another fault from the same dataset, lies towards the left-hand side of the plot with relatively lower proportions of strike relay zones and is adjacent to other points where a sequence control is clear. It may well be that there is a subtle variation in the sequence in the African Atlantic Margin dataset which impacts on fault propagation that is not recognised. Therefore, the group of faults identified as having no control (Fig. 11a) may incorporate faults where layering or structural inheritance controls are present but unidentified. While the data in Fig. 10 show systematic trends, albeit with large variability, it may well be that these trends would be much clearer if it was possible to identify more subtle effects.

The geometries mapped from seismic reflection data are at a particular scale and the controls attributed to them must act at that scale to be recognised. The geological controls we have highlighted may operate, or be absent, at scales both larger and smaller than those examined. For example, strong competence contrasts within a thinly bedded sequence (< 1 m) will not be reflected in the geometry of seismically imaged fault surfaces and the en-echelon arrangement of fault segments arising from pre-existing structural control may occur only at one scale and segmentation at smaller scales may not show the same consistency in stepping direction or increased proportion of strike relay zones. Despite the difficulties in objectively defining the controls operating on the geometry of fault surface, the scales at which they operate and the sampling biases as described in Section 4, our analysis of data from a range of settings has illustrated the wide range of fault surface geometry that occurs and has recognised systematic variations attributable to the properties of the faulted sequence and the influence of pre-existing structure.

7.3. Fault propagation

There are few geological constraints on the manner of fault surface propagation in 3D. One constraint that may be relevant is the 3D fault geometry insofar as cylindrical and bifurcating relay zones could be indicative of different modes of fault propagation. For example, it might be suggested that faults that are unconnected in 3D demonstrate fault surface growth by coalescence of initially isolated faults or that bifurcating geometries result from a single fault splitting into two lobes as it propagated, but alternative explanations have been proposed (Marchal et al., 2003; Conneally et al., 2014; Freitag et al., 2017). Here we have shown that, where sufficient data are available, individual faults comprise both forms of relay zone and individual faults contain segments that would have been initially unconnected and those with bifurcating geometries. The relative proportions of these two forms of relay zone vary according to geological setting leading to the conclusion that, although they have different geometries they do not represent fundamentally different modes of fault formation. Instead, the two relay forms are expressions of fault surface propagation, the details of which depend on geological controls that include the mechanical properties of the sequence and the presence of pre-existing structure or other causes of obliquity between the overall fault orientation and the orientation of the fault segments. We conclude that both fault bifurcation and stepping to form new unconnected segments are general modes of segmentation during fault propagation that vary according to geological setting and also potentially with scale.

8. Conclusions

Analysis of high-quality datasets highlights the broad variety of fault zone structure in three-dimensions. Faults exhibit a variety of geometries including individual fault surfaces bifurcating towards their tipline, faults initially comprising a patchwork of unconnected fault segments, and, most commonly, a complex combination of both these geometries. This fault zone complexity is accommodated by bifurcating and cylindrical relay zones developed in both strike and dip orientations. This variety has been examined in a compilation of faults from the literature and from newly-mapped seismic data, and attributed to the influence of geological controls, the impacts of resolution limit and biases on fault mapping from seismic data. When faults can be mapped in detail it appears that they contain a variety of relay zone types, but as data degrades and resolution decreases, strike and cylindrical relay zones appear to predominate. Pronounced mechanical layering promotes the formation of segmentation in the dip direction, with dip relay zones centred on weaker units, and may give rise to unconnected segments. For faults overlying a pre-existing structure, strike relay zones with a consistent sense of stepping are promoted. In the absence of mechanical heterogeneity these strike relay zones have a bifurcating form, but are more frequently cylindrical when mechanical heterogeneity is present. These geological controls define the dominant form or orientation of relay zones within a particular area but there is no reason to expect that any particular setting has exclusively one type of relay zone. Given a sufficient number of mapped relay zones, a wide variety of relay zone geometries are present, especially when no strong geological controls are apparent, and models of fault propagation should acknowledge that propagating faults can comprise segments that are both bifurcating and unconnected in three dimensions.

Declaration of Competing Interest

The authors declare that they have no known competing financial interests or personal relationships that could have appeared to influence the work reported in this paper.

Acknowledgements

This research was supported by a consortium-sponsored project brokered by the Industry Technology Facilitator, and funded by Anadarko, ConocoPhillips (UK), Eni, ExxonMobil, Equinor, Shell, Total E&P UK and Woodside Energy. This publication benefited from research supported in part by a research grant from Science Foundation Ireland (SFI) under Grant Number 13/RC/2092 and co-funded under the European Regional Development Fund and by PIPCO RSG and its member companies. Nagra (Swiss National Cooperative for the Disposal of Radioactive Waste) is thanked for providing access to seismic data. Badley Geoscience Ltd. is thanked for provision of T7 software licenses and Schlumberger for provision of Petrel software licenses. We thank the other members of the Fault Analysis Group for many useful discussions on the topic of this article, two anonymous reviewers for their useful comments and C. Doglioni for editorial handling.

References

Ackermann, R.V., Schlische, R.W., Withjack, M.O., 2001. The geometric and statistical evolution of normal fault systems: an experimental study of the effects of mechanical layer thickness on scaling laws. J. Struct. Geol. 23 (11), 1803–1819.

Badley, M.E., Freeman, B., Roberts, A.M., Thatcher, J.S., Walsh, J.J., Watterson, J., Yielding, G., 1990. Fault interpretation during seismic interpretation and reservoir evaluation. In: The Integration of Geology, Geophysics, Petrophysics and Petroleum Engineering in Reservoir Delineation, Description and Management. Proceedings of the 1st Archie Conference, Houston, Texas, Association of American Petroleum Geologists, pp. 224–241.

Baudon, C., Cartwright, J., 2008. Early stage evolution of growth faults: 3D seismic insights from the Levant Basin, Eastern Mediterranean. J. Struct. Geol. 30 (7), 888–898.

Bristol, H.M., Treworgy, J.D., 1979. The Wabash Valley Fault System in Southeastern Illinois. Circular no. 509.

Camanni, G., Roche, V., Childs, C., Manzocchi, T., Walsh, J., Conneally, J., Delogkos, E., 2019. The three-dimensional geometry of relay zones within segmented normal faults. Journal of Structural Geology 129, 103895.

Childs, C., Watterson, J., Walsh, J.J., 1995. Fault overlap zones within developing normal fault systems. J. Geol. Soc. 152 (3), 535–549.

Childs, C., Nicol, A., Walsh, J.J., Watterson, J., 1996a. Growth of vertically segmented normal faults. J. Struct. Geol. 18 (12), 1389–1397.

Childs, C., Watterson, J., Walsh, J.J., 1996b. A model for the structure and development of fault zones. J. Geol. Soc. 153 (3), 337–340.
Childs, C., Manzocchi, T., Nicol, A., Walsh, J.J., Soden, A.M., Conneally, J.C., Delogkos, E., 2017. The relationship between normal drag, relay ramp aspect ratio and fault zone structure. Geol. Soc. Lond., Spec. Publ. 439 (1), 355–372.
Clayton, L., 1966. Tectonic depressions along the Hope fault, a transcurrent fault in North Canterbury, New Zealand. N. Z. J. Geol. Geophys. 9 (1–2), 95–104.
Clifton, A.E., Schlische, R.W., Withjack, M.O., Ackermann, R.V., 2000. Influence of rift obliquity on fault-population systematics: results of experimental clay models. J. Struct. Geol. 22 (10), 1491–1509.
Collanega, L., Siuda, K., Jackson, C.A.L., Bell, R.E., Coleman, A.J., Lenhart, A., Breda, A., 2019. Normal fault growth influenced by basement fabrics: The importance of preferential nucleation from pre-existing structures. Basin Research 31 (4), 659–687.
Conneally, J., Childs, C., Walsh, J.J., 2014. Contrasting origins of breached relay zone geometries. J. Struct. Geol. 58, 59–68.
Conneally, J., Childs, C., Nicol, A., 2017. Monocline formation during growth of segmented faults in the Taranaki Basin, offshore New Zealand. Tectonophysics 721, 310–321.
Corti, G., 2008. Control of rift obliquity on the evolution and segmentation of the main Ethiopian rift. Nat. Geosci. 1 (4), 258.
Crider, J.G., Pollard, D.D., 1998. Fault linkage: three-dimensional mechanical interaction between echelon normal faults. J. Geophys. Res. Solid Earth 103 (B10), 24373–24391.
Das, S., Aki, K., 1977. Fault plane with barriers: a versatile earthquake model. J. Geophys. Res. 82 (36), 5658–5670.
Delogkos, E., Manzocchi, T., Childs, C., Camanni, G., Roche, V., 2020. The 3D structure of a normal fault from multiple outcrop observations. J. Struct. Geol. 104009.
Deng, H., McClay, K., 2019. Development of extensional fault and fold system: insights from 3D seismic interpretation of the Enderby Terrace, NW Shelf of Australia. Marine Petrol. Geol. 104, 11–28.
Deng, H., McClay, K., Bilal, A., 2020. 3D structure and evolution of an extensional fault network of the eastern Dampier Sub-basin, North West Shelf of Australia. J. Struct. Geol. 132, 103972.
Duffy, O.B., Bell, R.E., Jackson, C.A.L., Gawthorpe, R.L., Whipp, P.S., 2015. Fault growth and interactions in a multiphase rift fault network: Horda Platform, Norwegian North Sea. J. Struct. Geol. 80, 99–119.
Ferrill, D.A., Morris, A.P., 2003. Dilational normal faults. J. Struct. Geol. 25 (2), 183–196.
Ferrill, D.A., Morris, A.P., McGinnis, R.N., Smart, K.J., Watson-Morris, M.J., Wigginton, S.S., 2016. Observations on normal-fault scarp morphology and fault system evolution of the Bishop Tuff in the Volcanic Tableland, Owens Valley, California, USA. Lithosphere 8 (3), 238–253.
Ferrill, D.A., Morris, A.P., McGinnis, R.N., Smart, K.J., Wigginton, S.S., Hill, N.J., 2017. Mechanical stratigraphy and normal faulting. J. Struct. Geol. 94, 275–302.
Freitag, U.A., Sanderson, D.J., Lonergan, L., Bevan, T.G., 2017. Comparison of upwards splaying and upwards merging segmented normal faults. J. Struct. Geol. 100, 1–11.
Ghalayini, R., Homberg, C., Daniel, J.M., Nader, F.H., 2017. Growth of layer-bound normal faults under a regional anisotropic stress field. Geol. Soc. Lond., Spec. Publ. 439 (1), 57–78.
Giba, M., Walsh, J.J., Nicol, A., 2012. Segmentation and growth of an obliquely reactivated normal fault. J. Struct. Geol. 39, 253–267.
Goguel, J., 1952. Traité de tectonique. Masson, Paris.
Haghi, A.H., Kharrat, R., Asef, M.R., Rezazadegan, H., 2013. Present-day stress of the central Persian Gulf: implications for drilling and well performance. Tectonophysics 608, 1429–1441.
Huggins, P., Watterson, J., Walsh, J.J., Childs, C., 1995. Relay zone geometry and displacement transfer between normal faults recorded in coal-mine plans. J. Struct. Geol. 17 (12), 1741–1755.
Islam, M.S., Manzocchi, T., 2019. A novel flow-based geometrical upscaling method to represent three-dimensional complex sub-seismic fault zone structures into a dynamic reservoir model. Sci. Rep. 9 (1), 1–14.
Jackson, C.A.L., Rotevatn, A., 2013. 3D seismic analysis of the structure and evolution of a salt-influenced normal fault zone: a test of competing fault growth models. J. Struct. Geol. 54, 215–234.
Jackson, P., 1987. The corrugation and bifurcation of fault surfaces by cross-slip. J. Struct. Geol. 9 (2), 247–250.
Kattenhorn, S.A., Pollard, D.D., 2001. Integrating 3-D seismic data, field analogs, and mechanical models in the analysis of segmented normal faults in the Wytch Farm oil field, southern England, United Kingdom. AAPG Bull. 85 (7), 1183–1210.
Koledoye, B.A., Aydin, A., May, E., 2003. A new process-based methodology for analysis of shale smear along normal faults in the Niger Delta. AAPG Bull. 87 (3), 445–463.
Kristensen, M.B., Childs, C.J., Korstgård, J.A., 2008. The 3D geometry of small-scale relay zones between normal faults in soft sediments. J. Struct. Geol. 30 (2), 257–272.
Kyne, R., Torremans, K., Güven, J., Doyle, R., Walsh, J., 2019. 3-D Modeling of the Lisheen and Silvermines Deposits, County Tipperary, Ireland: Insights into Structural Controls on the Formation of Irish Zn-Pb Deposits. Econ. Geol. 114 (1), 93–116.
Läpädat, A., Imber, J., Yielding, G., Iacopini, D., McCaffrey, K.J., Long, J.J., Jones, R.R., 2017. Occurrence and development of folding related to normal faulting within a mechanically heterogeneous sedimentary sequence: a case study from Inner Moray Firth, UK. Geol. Soc. Lond., Spec. Publ. 439 (1), 373–394.
Larsen, P.H., 1988. Relay structures in a lower Permian basement-involved extension system, East Greenland. J. Struct. Geol. 10 (1), 3–8.
Laurent, D., Gay, A., Baudon, C., Berndt, C., Soliva, R., Planke, S., Lopez, M., 2012. High-resolution architecture of a polygonal fault interval inferred from geomodel applied to 3D seismic data from the Gjallar Ridge, Vøring Basin, Offshore Norway. Marine Geology 332, 134–151.
Long, J.J., Imber, J., 2011. Geological controls on fault relay zone scaling. J. Struct. Geol. 33 (12), 1790–1800.
Machette, M.N., Personius, S.F., Nelson, A.R., Schwartz, D.P., Lund, W.R., 1991. The Wasatch fault zone, Utah—Segmentation and history of Holocene earthquakes. J. Struct. Geol. 13 (2), 137–149.
Mandl, G., 1987. Discontinuous fault zones. J. Struct. Geol. 9 (1), 105–110.
Mandl, G., 2005. Rock Joints: The Mechanical Genesis. Springer-Verlag, Berlin Heidelberg (ISBN-10 3–340–24553-7).
Mansfield, C.S., Cartwright, J.A., 1996. High resolution fault displacement mapping from three-dimensional seismic data: evidence for dip linkage during fault growth. J. Struct. Geol. 18 (2–3), 249–263.
Manzocchi, T., Heath, A.E., Palananthakumar, B., Childs, C., Walsh, J.J., 2008. Faults in conventional flow simulation models: a consideration of representational assumptions and geological uncertainties. Pet. Geosci. 14 (1), 91–110.
Marchal, D., Guiraud, M., Rives, T., 2003. Geometric and morphologic evolution of normal fault planes and traces from 2D to 4D data. J. Struct. Geol. 25 (1), 135–158.
Marchant, R., Ringgenberg, Y., Stampfli, G., Birkhäuser, P., Roth, P., Meier, B., 2005. Paleotectonic evolution of the Zürcher Weinland (northern Switzerland), based on 2D and 3D seismic data. Eclogae Geol. Helv. 98 (3), 345–362.
McGrath, A.G., Davison, I., 1995. Damage zone geometry around fault tips. J. Struct. Geol. 17 (7), 1011–1024.
Micklethwaite, S., Ford, A., Witt, W., Sheldon, H.A., 2015. The where and how of faults, fluids and permeability–insights from fault stepovers, scaling properties and gold mineralisation. Geofluids 15 (1–2), 240–251.
Morley, C.K., 2017. The impact of multiple extension events, stress rotation and inherited fabrics on normal fault geometries and evolution in the Cenozoic rift basins of Thailand. Geol. Soc. Lond., Spec. Publ. 439 (1), 413–445.
Morley, C.K., Nelson, R.A., Patton, T.L., Munn, S.G., 1990. Transfer zones in the East African continental rift system and their relevance to hydrocarbon exploration in rifts (1). AAPG Bull. 74 (8), 1234–1253.
Muraoka, H., Kamata, H., 1983. Displacement distribution along minor fault traces. J. Struct. Geol. 5 (5), 483–495.
Nicol, A., Watterson, J., Walsh, J.J., Childs, C., 1996. The shapes, major axis orientations and displacement patterns of fault surfaces. J. Struct. Geol. 18 (2–3), 235–248.
Oglesby, D.D., 2020. What can Surface-Slip Distributions tell us about fault connectivity at depth? Bull. Seismol. Soc. Am. 110 (3), 1025–1036.
Peacock, D.C.P., 2002. Propagation, interaction and linkage in normal fault systems. Earth Sci. Rev. 58 (1–2), 121–142.
Peacock, D.C.P., 2003. Scaling of transfer zones in the British Isles. J. Struct. Geol. 25 (10), 1561–1567.
Peacock, D.C.P., Sanderson, D.J., 1991. Displacements, segment linkage and relay ramps in normal fault zones. J. Struct. Geol. 13 (6), 721–733.
Peacock, D.C.P., Sanderson, D.J., 1992. Effects of layering and anisotropy on fault geometry. J. Geol. Soc. 149 (5), 793–802.
Peacock, D.C.P., Sanderson, D.J., 1994. Geometry and development of relay ramps in normal fault systems. AAPG Bull. 78 (2), 147–165.
Peacock, D.C.P., Xing, Z., 1994. Field examples and numerical modelling of oversteps and bends along normal faults in cross-section. Tectonophysics 234 (1–2), 147–167.
Pizzi, A., Di Domenica, A., Gallovič, F., Luzi, L., Puglia, R., 2017. Fault segmentation as constraint to the occurrence of the main shocks of the 2016 Central Italy seismic sequence. Tectonics 36, 2370–2387.
Roche, V., Homberg, C., Rocher, M., 2012. Fault displacement profiles in multilayer systems: from fault restriction to fault propagation. Terra Nova 24 (6), 499–504.
Roche, V., Homberg, C., Rocher, M., 2013. Fault nucleation, restriction, and aspect ratio in layered sections: quantification of the strength and stiffness roles using numerical modeling. J. Geophys. Res. Solid Earth 118 (8), 4446–4460.
Roche, V., Childs, C., Madritsch, H., Camanni, G., 2020. Layering and structural inheritance controls on fault zone structure in three dimensions: a case study from the northern Molasse Basin, Switzerland. J. Geol. Soc. 177 (3)), 493–508.
Rotevatn, A., Fossen, H., 2011. Simulating the effect of subseismic fault tails and process zones in a siliciclastic reservoir analogue: Implications for aquifer support and trap definition. Mar. Pet. Geol. 28 (9), 1648–1662.
Rotevatn, A., Fossen, H., Hesthammer, J., Aas, T.E., Howell, J.A., 2007. Are relay ramps conduits for fluid flow? Structural analysis of a relay ramp in Arches National Park, Utah. Geol. Soc. Lond., Spec. Publ. 270 (1), 55–71.
Roth, F., Fleckenstein, P., 2001. Stress orientations found in north-East Germany differ from the west European trend. Terra Nova 13 (4), 289–296.
Rykkelid, E., Fossen, H., 2002. Layer rotation around vertical fault overlap zones: observations from seismic data, field examples, and physical experiments. Mar. Pet. Geol. 19 (2), 181–192.
Saqab, M.M., Bourget, J., 2015. Structural style in a young flexure-induced oblique extensional system, North-Western Bonaparte Basin, Australia. J. Struct. Geol. 77, 239–259.
Schöpfer, M.P.J., Childs, C., Walsh, J.J., 2006. Localisation of normal faults in multilayer sequences. J. Struct. Geol. 28, 816–833.
Schöpfer, M.P.J., Childs, C., Walsh, J.J., Manzocchi, T., Koyi, H.A., 2007. Geometrical analysis of the refraction and segmentation of normal faults in periodically layered sequences. J. Struct. Geol. 29, 318–335.
Schöpfer, M.P.J., Childs, C., Walsh, J.J., Manzocchi, T., 2016. Evolution of the internal structure of fault zones in three-dimensional numerical models of normal faults. Tectonophysics 666, 158–163.
Seebeck, H., Tenthorey, E., Consoli, C., Nicol, A., 2015. Polygonal faulting and seal integrity in the Bonaparte Basin, Australia. Mar. Pet. Geol. 60, 120–135.
Segall, P., Pollard, D.D., 1980. Mechanics of discontinuous faults. J. Geophys. Res. Solid Earth 85 (B8), 4337–4350.

Soliva, R., Schultz, R.A., Benedicto, A., 2005. Three-dimensional displacement-length scaling and maximum dimension of normal faults in layered rocks. Geophys. Res. Lett. 32 (16).
Soliva, R., Benedicto, A., Maerten, L., 2006. Spacing and linkage of confined normal faults: importance of mechanical thickness. J. Geophys. Res. Solid Earth 111 (B1).
Soliva, R., Benedicto, A., Schultz, R.A., Maerten, L., Micarelli, L., 2008. Displacement and interaction of normal fault segments branched at depth: Implications for fault growth and potential earthquake rupture size. J. Struct. Geol. 30 (10), 1288–1299.
Stein, R.S., Barka, A.A., Dieterich, J.H., 1997. Progressive failure on the North Anatolian fault since 1939 by earthquake stress triggering. Geophys. J. Int. 128 (3), 594–604.
Tingay, M., Bentham, P., De Feyter, A., Kellner, A., 2011. Present-day stress-field rotations associated with evaporites in the offshore Nile Delta. Bulletin 123 (5–6), 1171–1180.
Torabi, A., Alaei, B., Libak, A., 2019. Normal fault 3D geometry and displacement revisited: Insights from faults in the Norwegian Barents Sea. Mar. Pet. Geol. 99, 135–155.
Treagus, S.H., Lisle, R.J., 1997. Do principal surfaces of stress and strain always exist? J. Struct. Geol. 19 (7), 997–1010.
Trudgill, B., Cartwright, J., 1994. Relay-ramp forms and normal-fault linkages, Canyonlands National Park, Utah. Geol. Soc. Am. Bull. 106 (9), 1143–1157.
Tvedt, A.B., Rotevatn, A., Jackson, C.A.L., Fossen, H., Gawthorpe, R.L., 2013. Growth of normal faults in multilayer sequences: a 3D South China Seaase study from the Egersund Basin, Norwegian North Sea. J. Struct. Geol. 55, 1–20.
Vasquez, L., Nalpas, T., Ballard, J.F., Veslud, C.L.C.D., Simon, B., Dauteuil, O., Bernard, X.D., 2018. 3D geometries of normal faults in a brittle-ductile sedimentary cover: Analogue modelling. J. Struct. Geol. 112, 29–38.
Walsh, J.J., Watterson, J., 1990. New methods of fault projection for coalmine planning. In: Proceedings of the Yorkshire Geological Society, vol. 48, pp. 209–219.
Walsh, J.J., Watterson, J., Bailey, W.R., Childs, C., 1999. Fault relays, bends and branch-lines. J. Struct. Geol. 21 (8–9), 1019–1026.
Walsh, J.J., Bailey, W.R., Childs, C., Nicol, A., Bonson, C.G., 2003. Formation of segmented normal faults: a 3-D perspective. J. Struct. Geol. 25 (8), 1251–1262.
Walsh, J.J., Torremans, K., Güven, J., Kyne, R., Conneally, J., Bonson, C., 2018. Fault-controlled fluid flow within extensional basins and its implications for sedimentary rock-Hosted mineral deposits. Soc. Econ. Geol. Spec. Publ. 21, 237–269.
Watterson, J., Walsh, J.J., Gillespie, P.A., Easton, S., 1996. Scaling systematics of fault sizes on a large-scale range fault map. J. Struct. Geol. 18 (2–3), 199–214.
Wesnousky, S.G., 2008. Displacement and geometrical characteristics of earthquake surface ruptures: issues and implications for seismic-hazard analysis and the process of earthquake rupture. Bull. Seismol. Soc. Am. 98 (4), 1609–1632.
Wilkins, S.J., Gross, M.R., 2002. Normal fault growth in layered rocks at Split Mountain, Utah: influence of mechanical stratigraphy on dip linkage, fault restriction and fault scaling. J. Struct. Geol. 24 (9), 1413–1429.
Willemse, E.J., 1997. Segmented normal faults: Correspondence between three-dimensional mechanical models and field data. J. Geophys. Res. Solid Earth 102 (B1), 675–692.
Willemse, E.J., Pollard, D.D., 2000. Normal fault growth: evolution of tipline shapes and slip distribution. In: Aspects of Tectonic Faulting. Springer, Berlin, Heidelberg, pp. 193–226.
Wilson, P., Elliott, G.M., Gawthorpe, R.L., Jackson, C.A.L., Michelsen, L., Sharp, I.R., 2013. Geometry and segmentation of an evaporite-detached normal fault array: 3D seismic analysis of the southern Bremstein Fault complex, offshore mid-Norway. J. Struct. Geol. 51, 74–91.
Worthington, R.P., Walsh, J.J., 2017. Timing, growth and structure of a reactivated basin-bounding fault. Geol. Soc. Lond., Spec. Publ. 439 (1), 511–531.
Wrona, T., Magee, C., Jackson, C.A., Huuse, M., Taylor, K.G., 2017. Kinematics of polygonal fault systems: observations from the northern North Sea. Front. Earth Sci. 5, 101.